

1 A manuscript submitted to discussion forum of BG as a BG discussion paper(bg-2016-222):

2 **Revised according to the reviewer's comments (RC) 1**

3

4

5 Manganese and iron reduction dominate organic carbon oxidation in surface
6 sediments of the deep Ulleung Basin, East Sea

7

8

9 Jung-Ho Hyun^{1*}, Sung-Han Kim¹, Jin-Sook Mok¹, Hyeyoun Cho¹, Tongsup Lee², Verona
10 Vandieken³ and Bo Thamdrup^{4*}

11

12

13 ¹Department of Marine Sciences and Convergent Technology, Hanyang University, 55
14 Hanyangdaehak-ro, Ansan, Gyeonggi-do 15588, South Korea

15

16 ²Department of Oceanography, Pusan National University, Busan 609-735, South Korea

17

18 ³Institute for Chemistry and Biology of the Marine Environment, University of Oldenburg,
19 Carl-von-Ossietzky-Str. 9-11, 26129 Oldenburg, Germany

20

21 ⁴Nordic Center for Earth Evolution, Department of Biology, University of Southern Denmark,
22 Campusvej 55, 5230 Odense M, Denmark

23

24

25 *Correspondence to:

26 Jung-Ho Hyun (hyunjh@hanyang.ac.kr)

27 Bo Thamdrup (bot@biology.sdu.dk)

28

29

30

31 **Abstract.** Rates and pathways of benthic organic carbon (C_{org}) oxidation were investigated in
32 surface sediments of the Ulleung Basin (UB) characterized by high organic carbon contents ($>$
33 2.5 %, dry wt.) and very high contents of Mn oxides ($> 200 \mu\text{mol cm}^{-3}$) and Fe oxides (up to
34 $100 \mu\text{mol cm}^{-3}$). The combination of geochemical analyses and independently executed
35 metabolic rate measurements revealed that Mn and Fe reduction were the dominant C_{org}
36 oxidation pathways in the center of the UB, comprising 45 % and 20 % of total C_{org} oxidation,
37 respectively. By contrast, sulfate reduction was the dominant C_{org} oxidation pathway
38 accounting for 50 % of total C_{org} mineralization in sediments of the continental slope. The
39 relative significance of each C_{org} oxidation pathway matched the depth distribution of the
40 respective electron acceptors. The relative importance of Mn reduction for C_{org} oxidation
41 displays saturation kinetics with respect to Mn oxide content with a low half-saturation value
42 of $8.6 \mu\text{mol cm}^{-3}$, which further implies that Mn reduction can be a dominant C_{org} oxidation
43 process even in sediments with lower MnO_2 content as known from several other locations.
44 This is the first report of a high contribution of manganese reduction to C_{org} oxidation in
45 offshore sediments on the Asian margin. The high manganese oxide content in the surface
46 sediment in the central UB was maintained by an extreme degree of recycling, with each Mn
47 atom on average being reoxidized ~ 3800 times before permanent burial. This is the highest
48 degree of recycling so far reported for Mn-rich sediments, and it appears linked to the high
49 benthic mineralization rates resulting from the high organic carbon content that indicate the
50 UB as a biogeochemical hotspot for turnover of organic matter and nutrient regeneration.
51 Thus, it is important to monitor any changes in the rates and partitioning of C_{org} oxidation to
52 better understand the biogeochemical cycling of carbon, nutrients and metals associated with
53 long-term climatic changes in the UB, where the gradual deoxygenation and warming of the
54 bottom water have resulted in an ~ 10 % decrease in dissolved oxygen and ~ 0.04 °C
55 increase in potential temperature for the past three decades.

56
57

58 **Keywords.** Benthic mineralization, Manganese reduction, Iron reduction, Sulfate reduction,
59 Ulleung Basin, East Sea

60
61
62
63

64 **1 Introduction**

65

66 Although they cover only 15 % ($47 \times 10^6 \text{ km}^2$) of the ocean surface area, sediments of
67 continental margins (200 – 2000 m depth) are characterized by enhanced organic matter flux
68 generated either by vertical transport from the highly productive overlying water column or
69 by lateral transport from adjacent shelves, and thus play an important role in deposition and
70 mineralization of organic matter (Romankevich, 1984, Jahnke et al., 1990; Walsh, 1991;
71 Jahnke and Jahnke, 2000). Organic particles that reach the seafloor are quickly mineralized
72 by hydrolysis, fermentation, and a variety of respiratory processes using different electron
73 acceptors such as oxygen, nitrate, Mn oxides, Fe oxides, and sulfate (Froelich et al., 1979;
74 Jørgensen, 2006). The partitioning of organic carbon (C_{org}) oxidation among the different
75 electron accepting pathways has profound influence on the distribution and the release and/or
76 retention of Mn, Fe, S and nutrients (nitrogen and phosphate) (Canfield et al., 2005; Hansen
77 et al., 2006; Jørgensen, 2006; Slomp et al., 2013). Therefore, it is particularly important to
78 elucidate the contribution of each C_{org} oxidation pathway in order to better understand the
79 role of sediments in biogeochemical element cycles.

80 The relative significance of each carbon oxidation pathway is largely controlled by the
81 combination of organic matter supply and availability of electron acceptors. In general,
82 aerobic metabolism dominates the organic matter mineralization in deep-sea sediments that
83 are characterized by low organic matter content (Jahnke et al., 1982; Glud, 2008), especially
84 in organic carbon-starved deep-sea sediments with low sedimentation rates (Mewes et al.,
85 2014, 2016; D'Hondt et al. 2015; Mogollón et al., 2016). In contrast, owing to high sulfate
86 concentrations in marine sediment, sulfate reduction might account for up to 50 % of total
87 carbon oxidation in continental margins with high organic matter flux (Jørgensen, 1982;
88 Jørgensen and Kasten, 2006; Bowles et al., 2014). However, in sediments where manganese
89 and iron oxides are abundant or rapidly recycled, microbial reduction of manganese and iron
90 can be the dominant electron accepting processes over sulfate reduction (Sørensen and
91 Jørgensen, 1987; Aller, 1990; Canfield et al., 1993b). The significance of dissimilatory iron
92 reduction for C_{org} oxidation is well established in the sediments of various continental
93 margins and coastal wetlands (Thamdrup, 2000; Thamdrup and Canfield, 1996; Jensen et al.
94 2003, Kostka et al., 2002a, 2002b; Vandieken et al., 2006; Hyun et al., 2007, 2009b).
95 However, only a few locations such as the Panama Basin (Aller, 1990), the coastal
96 Norwegian trough in Skagerrak and an adjacent fjord (Canfield et al., 1993a, 1993b;

97 Vandieken et al., 2014), the Black Sea shelf (Thamdrup et al., 2000) and the continental shelf
98 of the northern Barents Sea (Vandieken et al., 2006; Nickel et al., 2008) are known where
99 microbial manganese reduction significantly contributes to carbon mineralization.

100 The East Sea (often referred to as Japan Sea), located in the far eastern part of the Eurasian
101 continental margin, consists of three major basins deeper than 2000 m, the Japan Basin, the
102 Yamato Basin and the Ulleung Basin (Fig. 1). Compared to the other two basins, the surface
103 waters of the Ulleung Basin (UB) are characterized by higher phytoplankton biomass and
104 primary production (Yamada et al., 2005; Yoo and Park, 2009), which is associated with
105 coastal upwelling (Hyun et al., 2009a). The enhanced biological production in the euphotic
106 zone of the UB is responsible for the high organic carbon content (> 2.5 % wt) in the
107 sediment, and the highest rates of C_{org} oxidation compared to other deep-sea sediments with
108 similar depth range (Lee et al., 2008; Hyun et al., 2010). An intriguing geochemical property
109 of the UB surface sediment is the high content of Mn oxides ($>200 \mu\text{mol cm}^{-3}$) and Fe oxides
110 (up to $100 \mu\text{mol cm}^{-3}$) (Cha et al., 2007; Hyun et al., 2010). In accordance with these
111 geochemical findings, the suppression of sulfate reduction (Hyun et al., 2010) and
112 accumulation of Mn^{2+} in anoxic incubation of surface sediment (Vandieken et al., 2012)
113 strongly implied that the C_{org} oxidation in the surface sediment of the UB is dominated by
114 microbial manganese and iron reduction, but actual rates and partitioning of each electron
115 accepting pathway in C_{org} oxidation remain to be determined in this deep marginal sediment
116 underlying highly productive surface waters.

117 The primary objective of this paper was to characterize the sediment biogeochemistry with
118 regard to the rate of C_{org} oxidation and partitioning of major terminal electron accepting
119 pathways at two contrasting sites at the continental slope and rise in the UB. Here, for the
120 first time in sediments of the Asian marginal seas, we document that Mn and Fe reduction are
121 the dominant C_{org} oxidation pathways accounting for respectively 45 % and 20 % of total C_{org}
122 oxidation in the center of the UB, and suggest that Mn and Fe reduction may be of greater
123 importance in deep-sea sediments than previously recognized.

124

125 **2 Materials and methods**

126

127 **2.1 Study site**

128

129 The East Sea is a marginal sea surrounded by the east Asian continent and Japanese Islands

130 (Fig.1, Kang et al., 2010; Liu et al., 2010). The UB located in the southwestern part of the
131 East Sea is a bowl-shaped deep basin (2000 – 3000 m depth) (Fig. 1) delimited by continental
132 slopes of Korean Peninsula and the southwestern Japanese Archipelago on the west and south,
133 respectively, and by the Korea Plateau and the Oki Bank on the north and east, respectively
134 (Chough et al., 2000).

135 Shipboard experiments were conducted in June, 2009 at two sites on the continental slope
136 (Station M1, hereafter M1) and in the center (Station D3, hereafter D3) of the the UB (Fig. 1,
137 Table 1). Surface sediments consist of fine-grained clay with a mean grain size less than
138 0.004 mm in diameter (Cha et al., 2007). Two stations were characterized by two contrasting
139 sediment colors. The Mn oxide-enriched surface sediment at the basin site (D3) was reddish-
140 brown, whereas at the slope site (M1) it exhibited the typical gray-brown color of muddy
141 continental margin sediments (Fig. 1). Further environmental properties are listed in Table 1.

142

143 **2.2 Sampling and handling**

144

145 Sediment samples were collected with a box corer. Onboard, duplicate or mostly triplicate
146 sub-samples for geochemical analyses were collected using acrylic cores (6–9 cm in diameter
147 and 30–40 cm in length). The sub-cores for geochemical analyses were immediately sealed
148 with butyl rubber stoppers and transferred to a N₂-filled glove bag for sectioning and loading
149 into polypropylene centrifuge tubes that were then tightly capped and centrifuged for 15 min
150 at 5000 × g. After reintroduction into the N₂-filled glove bag, pore-waters were sampled and
151 filtered through 0.2-μm cellulose ester syringe filters (ADVANTEC, Toyo Rashi Kaisha, Ltd).
152 One to two mL of pore water to determine NH₄⁺ was fixed with saturated HgCl₂, and frozen.
153 For determination of Fe²⁺, Mn, SO₄²⁻ and Ca²⁺, 2 mL of the pore water were acidified with
154 12M HCl and stored at 4 °C. Pore-water for sulfide analysis was preserved with Zn acetate
155 (20 %). Sediments for solid-phase analysis were frozen at –25°C for future analyses.

156

157 **2.3 Anoxic bag incubations**

158

159 Anaerobic carbon mineralization rates and dissimilatory Mn and Fe reduction rates were
160 determined in batch incubations based on the procedures of Canfield et al. (1993b) and
161 Thamdrup and Canfield (1996). Sediment cores were transferred to a N₂-filled glove bag and
162 sliced in 2-cm intervals to a depth of 10 cm. Sediment from parallel sections was pooled,

163 mixed and loaded into gas-tight plastic bags (Hansen et al., 2000). The bags were sealed
164 without gas space, and incubated in the dark at near in situ temperature (ca. 1–2°C) in larger
165 N₂ filled bags to ensure anoxic conditions. Over a period of 18 days of incubation, sub-
166 samples to determine the accumulation of total dissolved inorganic carbon (DIC) and Mn in
167 pore water were withdrawn on days 0, 1, 3, 5, 9 and 18. Two 50-mL centrifuge tubes per bag
168 were filled completely with sediment in a N₂-filled glove bag, and pore-water was extracted
169 as described above. For DIC analysis, we collected 1.8 mL aliquots into glass vials without
170 head space, fixed with 18 µL of HgCl₂ (125 mM), and stored at 4 °C until analysis within 4
171 weeks. Samples for Mn analysis were acidified with 12 M HCl and stored at 4°C. Sediment
172 remaining after the collection of pore water was frozen at –25°C for later analysis of oxalate
173 extractable solid Fe(II).

174

175 **2.4 Pore-water analyses**

176

177 Total dissolved inorganic carbon (DIC) and NH₄⁺ were measured by flow injection analysis
178 with conductivity detection (Hall and Aller, 1992). Nitrate was measured
179 spectrophotometrically (Parsons et al., 1984). Dissolved Fe²⁺ was determined by colorimetric
180 method with Ferrozine (Stookey, 1970). Dissolved Mn²⁺ and Ca²⁺ were analyzed in acidified
181 pore water by inductively coupled plasma-atomic emission spectrometry (ICP-AES, Optima
182 3300DV, Perkin-Elmer Co.) and flame atomic absorption spectrometer (SpectrAA 220/FS,
183 Varian), respectively (Thamdrup and Canfield, 1996). Dissolved sulfide was determined by
184 the methylene blue method (Cline, 1969). Sulfate concentrations were measured using ion
185 chromatography (Metrohm 761). The detection limit of H₂S, Ca²⁺, Mn²⁺ and Fe²⁺ was 3 µM,
186 1.8 µM, 3 µM and 1 µM, respectively. Reproducibility of DIC and NH₄⁺ was better than 10%.
187 Precision of NO₃⁻ was 1 – 2%.

188

189 **2.5 Solid-phase analyses**

190

191 Total oxalate-extractable Fe [Fe(II) + Fe(III)] was extracted from air-dried sediment in a 0.2
192 M oxalic acid solution (pH 3) for 4 h (Thamdrup and Canfield, 1996), and Fe(II) was
193 extracted from frozen sediment in anoxic oxalate (Phillips and Lovley, 1987). The total
194 oxalate-extractable Fe and Fe(II), hereafter total Fe_(oxal) and Fe(II)_(oxal), were determined as
195 described for the pore-water analysis of Fe²⁺. Oxalate-extractable Fe(III), hereafter

196 Fe(III)_(oxal), was defined as the difference between total Fe_(oxal) and Fe(II)_(oxal). This fraction
197 represents poorly crystalline Fe(III) oxides. Particulate Mn, hereafter Mn_(DCA) was extracted
198 with dithionite-citrate-acetic acid (DCA; pH 4.8) for 4 h from air-dried sediment and was
199 determined by inductively coupled plasma-atomic emission spectrometry (ICP-AES, Optima
200 3300DV, Perkin-Elmer Co). The DCA extraction aims at dissolving free Mn oxides and
201 authigenic Mn(II) phases. The reproducibility of the measurements was better than 10% and
202 the detection limits was 3 μM for Mn and 1 μM for Fe. For the determination of total reduced
203 sulfur (TRS) that includes acid volatile sulfide (AVS = FeS + H₂S and small amounts of other
204 metal sulfides, see Rickard and Morse, 2005; Luther, 2005) and chromium-reducible sulfur
205 (CRS = S⁰ + FeS₂), sediment samples were fixed with Zn acetate, and sulfide was determined
206 according to the method of Cline (1969) after a two-step distillation with cold 12 M HCl and
207 boiling 0.5 M Cr²⁺ solution (Fossing and Jørgensen, 1989). The contents of particulate
208 organic carbon (POC) and nitrogen (PON) in the surface sediment were analyzed using a
209 CHN analyzer (CE Instrument, EA 1110) after removing CaCO₃ using 12 M HCl.

210

211 **2.6 Oxygen micro-profiles**

212

213 Oxygen profiles were measured at 50 μm resolution using Clark-type microelectrodes
214 (Unisense, OX-50) while stirring the overlying water. Microelectrodes were calibrated
215 between 100% air-saturated *in situ* bottom water and N₂ purged anoxic bottom water. Three
216 profiles were measured at each site. The diffusive boundary layer (DBL) and sediment-water
217 interface (SWI) were determined according to Jørgensen and Revsbech (1985). To estimate
218 the volume-specific oxygen consumption rate, we used the PROFILE software (Berg et al.,
219 1998).

220

221 **2.7 Rate measurements**

222

223 The diffusive oxygen uptake (DOU) was calculated from the calibrated oxygen microprofiles.

224

$$225 \text{DOU} = -D_o \Delta C / \Delta z, \quad (1)$$

226

227 where D_o ($1.07 \times 10^{-9} \text{ m}^2 \text{ s}^{-1}$ at M1 and $1.03 \times 10^{-9} \text{ m}^2 \text{ s}^{-1}$ at D3) is the temperature-corrected
228 molecular diffusion coefficient estimated from Schulz (2006), and C is the oxygen

229 concentration at depth z within the diffusive boundary layer (DBL) (Jørgensen and Revsbech,
230 1985).

231 The volume-specific O_2 consumption rates exhibited a bimodal depth distribution (see
232 results section 3.2) with activity peaks near the sediment-water interface and the oxic/anoxic
233 interface, respectively. Thus, O_2 consumption rates by aerobic organotrophic respiration was
234 defined as the O_2 consumption rate near the sediment-water interface, whereas the oxygen
235 consumption at the oxic-anoxic interface was assigned to re-oxidation of reduced inorganic
236 compounds (Rasmussen and Jørgensen, 1992; Canfield et al., 2005).

237 Total anaerobic C_{org} mineralization rates were determined by linear regression of the
238 accumulation of total DIC with time during the anoxic bag incubations (Fig. 3) after
239 correcting for $CaCO_3$ precipitation (Thamdrup et al., 2000). Briefly, $CaCO_3$ precipitation was
240 calculated from decreasing dissolved Ca^{2+} concentration during the anoxic bag incubation:

241

$$242 \Delta CaCO_3 = \Delta [Ca^{2+}]_{sol} \times (1 + K_{Ca}), \quad (2)$$

243

244 where, K_{Ca} is the adsorption constant for Ca^{2+} ($K_{Ca} = 1.6$) (Li and Gregory, 1974). Then rate
245 of DIC production rate corrected for $CaCO_3$ precipitation was calculated as:

246

$$247 \text{DIC production} = \text{DIC accumulation} + CaCO_3 \text{ precipitation} \quad (3)$$

248

249 Fe(III) reduction rates were determined by linear regression of the increase in solid-phase
250 Fe(II)_(oxal) content with time during anoxic bag incubations. The dissimilatory microbial Fe(III)
251 reduction rate was derived by subtracting abiotic Fe reduction coupled to the oxidation of
252 sulfide produced by sulfate reduction (Gribsholt et al. 2003):

253

$$254 \text{Dissimilatory microbial Fe(III) Red} = \text{Total Fe(III) Red} - \text{Abiotic Fe(III) Red} \quad (4)$$

255

256 assuming that abiotic Fe reduction coupled to H_2S oxidation occurred at a stoichiometry of 2
257 Fe(III) per 3 H_2S (Pyzik and Sommer, 1981; Melton et al., 2014):

258

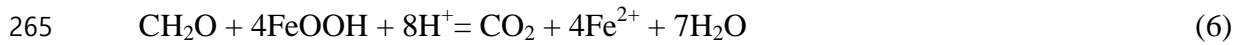


260

261 Finally, to estimate the C_{org} oxidation by microbial Fe reduction, the 4:1 stoichiometry of

262 iron reduction coupled to C_{org} oxidation was used from the stoichiometric equation (Canfield
263 et al., 1993a):

264



266

267 Mn reduction rates were determined from linear regression of the production of dissolved
268 Mn²⁺ with time during the anoxic bag incubations. Similar to previous studies (e.g., Canfield
269 et al., 1993a, 1993b; Thamdrup and Dalsgaard, 2000), we assumed that accumulating
270 dissolved Mn was Mn²⁺. This ignores a potential contribution from Mn³⁺, which in some
271 cases can constitute a substantial fraction of the dissolved Mn pool at the upper boundary of
272 the zone with soluble Mn accumulation in marine sediments (Madison et al., 2013). Further
273 studies of the dynamics of soluble Mn³⁺ are required to evaluate its potential importance in
274 anoxic incubations. Such studies pending, we find justification for our assumption in the
275 good agreement observed in the previous studies between Mn reduction rates calculated
276 based on the assumption that soluble Mn is Mn²⁺ (Eq. 7) and independent estimates of rates
277 of carbon mineralization through dissimilatory Mn reduction based on DIC or NH₄⁺
278 accumulation. Due to strong adsorption of Mn²⁺ to Mn oxide surfaces (Canfield et al., 1993b),
279 the Mn reduction rates were estimated after compensating for the adsorption effect of Mn²⁺ to
280 Mn-oxides according to Thamdrup and Dalsgaard (2000):

281

$$282 \quad \text{Mn reduction rate} = \text{Mn}^{2+} \text{ accumulation rate} \times (1 + K_{\text{Mn}}^* \times (1 - \Phi) \times \Phi^{-1} \times \delta_s) \quad (7)$$

283

284 where, Φ = porosity

285 δ_s = density of sediment

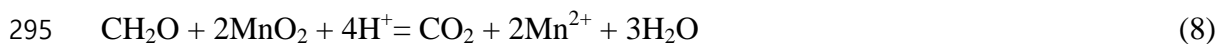
$$286 \quad K_{\text{Mn}}^* = 4.8 + 0.14 \times [\text{Mn(IV)}] \text{ (ml g}^{-1}\text{)}$$

$$287 \quad [\text{Mn(IV)}] = \text{the content of Mn(IV) (}\mu\text{mol g}^{-1}\text{)}$$

288

289 We here assume that extracted Mn_(DCA) represents Mn(IV) as observed in surface
290 sediments of another Mn-rich site (Canfield et al., 1993b, Thamdrup and Dalsgaard, 2000).
291 Small levels of Mn_(DCA) remaining at depth further suggest that little Mn(II) accumulates in
292 the solid phase (*see* Results). C_{org} oxidation by dissimilatory Mn(IV) reduction was
293 calculated from the stoichiometric equation (Canfield et al., 1993a):

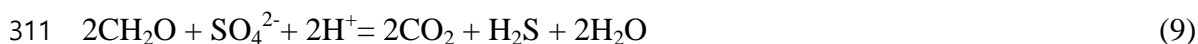
294



296

297 Sulfate reduction rates were determined using the radiotracer method of Jørgensen (1978).
298 Sediment cores (35 cm long with 2.9 cm i.d.) were collected in triplicate, injected
299 horizontally at 1-cm vertical interval with 5 μL radiolabeled sulfate ($^{35}\text{S}\text{-SO}_4^{2-}$, 15 kBq μL^{-1} ,
300 Amersham) diluted in sterilized NaCl solution (3.0 %), and incubated for 12 h at *in situ*
301 temperature. At the end of the incubation, the sediment was sliced into sections, fixed in Zn
302 acetate (20 %), and frozen at -25°C until processed in the laboratory. The reduced ^{35}S was
303 recovered using distillation with a boiling acidic Cr^{2+} solution according to Fossing and
304 Jørgensen (1989). Background radioactivity of ^{35}S was 32.4 ± 3.7 cpm cm^{-3} ($n=10$) at site D3
305 and 87.5 ± 38.7 cpm cm^{-3} ($n=10$) at site M1. Detection limits of the SRR, estimated from the
306 double standard deviation of the blank value (i.e., 7.4 and 77.4 cpm) according to Fossing et
307 al. (2000), ranged from 0.79 to 2.62 $\text{nmol cm}^{-3} \text{d}^{-1}$. To elucidate the contribution of sulfate
308 reduction in anaerobic carbon oxidation, the SRRs (Fig. 5B, 5G) were converted to carbon
309 oxidation using a stoichiometric equation (Thamdrup and Canfield, 1996):

310



312

313 **3 Results**

314

315 **3.1 Pore-water and solid-phase constituents**

316

317 The depth distributions of NH_4^+ , NO_3^- , Mn^{2+} and Fe^{2+} in the pore-water as well as solid phase
318 Mn, Fe and S for the two stations are shown in Fig. 2. NH_4^+ concentrations at M1 increased
319 steadily with depth (Fig. 2A) whereas at D3 it decreased down to 3 cm depth before it
320 increased below (Fig. 2F). Highest concentrations of nitrate were measured at 0 to 1 cm
321 sediment depth at the two stations and concentrations decreased below a background level ($<$
322 $2 \mu\text{M}$) below 1 cm at both M1 and D3 (Fig. 2A, 2F). Dissolved Mn^{2+} concentrations differed
323 widely between the sites showing a maximum of 56 μM between 0 and 3 cm depth and not
324 exceeding 10 μM below at M1 (Fig. 2B), whereas at D3 concentrations increased to a
325 maximum of 286 μM at 10 – 12 cm depth (Fig. 2G). Conversely, dissolved Fe^{2+}

326 concentrations at M1 increased from 11 μM at 0 – 0.5 cm to 32 μM at 6 – 7 cm depth, and
327 stayed constant below (Fig. 2C), whereas at D3, concentrations were uniformly low showing
328 a slight increase to 12 μM at 15 cm (Fig. 2F).

329 Extractable Mn ($\text{Mn}_{(\text{DCA})}$) contents were low ($< 3 \mu\text{mol cm}^{-3}$) in the upper 20 cm at the
330 slope site (M1) (Fig. 2B), but up to 200 $\mu\text{mol cm}^{-3}$ in the upper 4 cm depth of the sediment at
331 the center of the basin (D3), with a sharp decrease to near depletion ($\sim 1 \mu\text{mol cm}^{-3}$) below 10
332 cm (Fig. 2G). At the slope site (M1), contents of $\text{Fe}(\text{III})_{(\text{oxal})}$ decreased slightly with
333 increasing depth from 28 $\mu\text{mol cm}^{-3}$ near the surface to 13 $\mu\text{mol cm}^{-3}$ at 20 cm depth,
334 mirroring an increase in $\text{Fe}(\text{II})_{(\text{oxal})}$ (Fig. 2D). At the center of the basin (D3), $\text{Fe}(\text{III})_{(\text{oxal})}$
335 increased slightly from 67 $\mu\text{mol cm}^{-3}$ at 0 – 0.5 cm to 90 $\mu\text{mol cm}^{-3}$ at 4 – 6 cm depth, and
336 decreased steeply below to 4.8 $\mu\text{mol cm}^{-3}$ at 12 – 14 cm depth (Fig. 2I). Of total $\text{Fe}_{(\text{oxal})}$,
337 $\text{Fe}(\text{III})_{(\text{oxal})}$ comprised $> 98 \%$ at 0 – 2 cm and $> 97 \%$ at 0 – 8 cm depth at M1 and D3,
338 respectively. The fraction of $\text{Fe}(\text{III})_{(\text{oxal})}$ in $\text{Fe}_{(\text{oxal})}$ then decreased to 40 % at 10 – 12 cm depth
339 at both sites. Acid volatile sulfur (AVS) exhibited a slight increase with depth at M1 from 0.8
340 $\mu\text{mol cm}^{-3}$ at the surface to 7.2 $\mu\text{mol cm}^{-3}$ at 20 cm depth (Fig. 2E), but was not detected at
341 D3 (Fig. 2J). Chromium reducible sulfur (CRS) contents at M1 increased rapidly with depth
342 from 1.9 $\mu\text{mol cm}^{-3}$ at 0 – 0.5 cm to 21.8 $\mu\text{mol cm}^{-3}$ at 20 cm depth (Fig. 2D), whereas the
343 CRS contents remained $< 0.1 \mu\text{mol cm}^{-3}$ at D3 (Fig. 2J).

344

345 **3.2 O₂ microprofiles and diffusive oxygen uptake rate**

346

347 Oxygen penetrated less than 4 mm into the sediments (Fig. 3), and rates of diffusive oxygen
348 uptake (DOU) were 7.1 and 6.0 $\text{mmol O}_2 \text{ m}^{-2} \text{ d}^{-1}$ at M1 and D3, respectively (Table 2).
349 Oxygen consumption by aerobic respiration estimated from the O₂ micro-profiles (area I and
350 II in Fig. 3) was higher at the M1 in the slope site (4.0 $\text{mmol O}_2 \text{ m}^{-2} \text{ d}^{-1}$) than at the D3 in the
351 center of the basin (2.5 $\text{mmol O}_2 \text{ m}^{-2} \text{ d}^{-1}$). O₂ consumption by re-oxidation of reduced
352 inorganic compounds indicated by increased activity at the oxic/anoxic interface (area III in
353 Fig. 3) accounted for 43 % and 57 % of the DOU at M1 and D3, respectively. From the
354 profiles of geochemical constituents (Fig. 2), O₂ consumption was mainly attributed to the re-
355 oxidation of sulfide and Fe^{2+} at M1 and of Mn^{2+} at D3.

356

357 **3.3 Anoxic bag incubations**

358

359 Changes in concentrations of DIC, Ca^{2+} and dissolved Mn^{2+} and solid $\text{Fe(II)}_{(\text{oxal})}$ contents
360 over time during anoxic bag incubations from sediment of 0 – 2, 2 – 4, 4 – 6 and 6 – 8 cm
361 depth intervals are presented in Fig. 4. The DIC concentrations increased linearly over time
362 during incubations of sediment in all bags from M1 and D3, except the bag from 6 – 8 cm at
363 D3. The DIC accumulation rates were generally higher at the slope site (M1) than at the basin
364 site (D3) (Table 4). The concentrations of Ca^{2+} decreased with time at all depth intervals of
365 M1, whereas a decrease of Ca^{2+} was observed only for the 2 – 4 cm depth interval at D3. The
366 decrease of Ca^{2+} indicates CaCO_3 precipitation, which consequently underestimates DIC
367 accumulation, especially at M1.

368 Coinciding with high solid $\text{Mn}_{(\text{DCA})}$ contents (Fig. 2G), prominent Mn^{2+} accumulation
369 appeared at 0 – 6 cm depth of D3, whereas no increase of Mn^{2+} was observed at M1 except a
370 slight accumulation at 0 – 2 cm interval (Fig. 4). Solid $\text{Fe(II)}_{(\text{oxal})}$ contents increased linearly
371 with time at 0 – 4 cm depth of M1, whereas highest $\text{Fe(II)}_{(\text{oxal})}$ accumulation was observed at
372 4 – 6 cm depth at D3. An increase of $\text{Fe(II)}_{(\text{oxal})}$ was not discernible in the Mn-oxide-rich
373 surface sediment (0 – 2 cm) of D3.

374

375 **3.4 Sulfate reduction rates (SRR)**

376

377 At the slope site (M1), SRR increased from $18 \text{ nmol cm}^{-3} \text{ d}^{-1}$ at the surface to $97 - 103 \text{ nmol}$
378 $\text{cm}^{-3} \text{ d}^{-1}$ at 1.5 – 2 cm depth, and decreased below to $12.5 \text{ nmol cm}^{-3} \text{ d}^{-1}$ at 20 cm depth (Fig.
379 5B). In contrast, SRR at the manganese oxide-rich basin site (D3) ranged from 1.7 to 8.7
380 $\text{nmol cm}^{-3} \text{ d}^{-1}$, and did not vary with depth. Depth integrated SRR down to 10 cm depth was
381 10 times higher at M1 ($4.3 \text{ mmol m}^{-2} \text{ d}^{-1}$) than at D3 ($0.4 \text{ mmol m}^{-2} \text{ d}^{-1}$) (Table 3).

382

383 **3.5 DIC production rates**

384

385 Vertical profiles of the DIC production rate that were derived from the linear regression of
386 the DIC production measured in anoxic bag incubation (Fig. 4) after correcting for CaCO_3
387 precipitation, are presented in Fig. 5C and 5H for M1 and D3, respectively. At M1, the DIC
388 production rates decreased with depth from $280 \text{ nmol cm}^{-3} \text{ d}^{-1}$ (0 – 2 cm depth) to 69 nmol
389 $\text{cm}^{-3} \text{ d}^{-1}$ (8 – 10 cm depth) (Fig. 5C), whereas the DIC production rates at D3 were relatively
390 similar across the upper 6 cm ranging from 86 to $136 \text{ nmol cm}^{-3} \text{ d}^{-1}$, and decreased to 8 – 15
391 $\text{nmol cm}^{-3} \text{ d}^{-1}$ at 6– 10 cm (Fig. 5H). The integrated DIC production rate within 10 cm depth

392 of the sediment was twice as high at M1 ($14.0 \text{ mmol m}^{-2} \text{ d}^{-1}$) as at the D3 ($7.2 \text{ mmol m}^{-2} \text{ d}^{-1}$)
393 (Table 4).

394

395 **3.6 Rates of Mn and Fe reduction**

396

397 The accumulation of Mn^{2+} presented evidence that manganese reduction was occurring in the
398 surface sediment (0 – 6 cm) of D3 (Fig. 4). The manganese reduction rate (MnRR) derived
399 from Mn^{2+} accumulation with correction for adsorption ranged from $7.5 \text{ nmol cm}^{-3} \text{ d}^{-1}$ (0 – 2
400 cm depth) to $198 \text{ nmol cm}^{-3} \text{ d}^{-1}$ (2 – 4 cm depth) at D3 (Fig. 5I). In contrast, MnRR at M1
401 was indiscernible except for low activity ($2.2 \text{ nmol cm}^{-3} \text{ d}^{-1}$) at 0 – 2 cm depth (Fig. 5D).
402 Depth integrated MnRR at D3 ($8.21 \text{ mmol m}^{-2} \text{ d}^{-1}$) was 200 times higher than the MnRR at
403 M1 ($0.04 \text{ mmol m}^{-2} \text{ d}^{-1}$) (Table 3). The iron reduction rate (FeRR), derived from $\text{Fe(II)}_{(\text{oxal})}$
404 accumulation, at M1 was highest in the 0 – 2 cm interval ($237 \text{ nmol cm}^{-3} \text{ d}^{-1}$), and then
405 decreased with depth to $38 \text{ nmol cm}^{-3} \text{ d}^{-1}$ at 8 – 10 cm depth (Fig. 5E). In contrast, Fe
406 reduction was not detected in the surface sediment at D3, but increased to its maximum rate
407 of $240 \text{ nmol cm}^{-3} \text{ d}^{-1}$ at 4 – 6 cm depth. The FeRR then decreased with depth to 12 nmol cm^{-3}
408 d^{-1} at 8 – 10 cm (Fig. 5J) where a few data points were adopted to derive the line of best-fit
409 regression. Depth integrated total FeRR was slightly higher at M1 ($11.4 \text{ mmol m}^{-2} \text{ d}^{-1}$) than at
410 D3 ($7.53 \text{ mmol m}^{-2} \text{ d}^{-1}$) (Table 3). The ratio of microbial Fe reduction, $\text{Fe Red}_{(\text{microbial})}$, to
411 abiotic Fe reduction coupled to sulfide oxidation, $\text{Fe Red}_{(\text{abiotic})}$, ranged from 1.14 (8 – 10 cm
412 at M1) to 52.3 (2 – 4 cm at D3), which indicated that the Fe reduction at Mn- and Fe oxides
413 rich basin site was mostly a microbiologically mediated process (Table 3).

414

415 **4 Discussion**

416

417 **4.1 Partitioning of C_{org} oxidation in accordance with the distribution of terminal** 418 **electron acceptors**

419

420 One of the most prominent features revealed from the vertical distributions of geochemical
421 constituents at the basin site (D3) was that electron acceptors such as O_2 , nitrate, Mn- and Fe
422 oxides were systematically distributed with discrete zonation according to the order of
423 decreasing energy yield for C_{org} oxidation (Fig. 5F). Such biogeochemical zones are not
424 sharply separated in most aquatic sediments due to, e.g., sediment heterogeneity and mixing

425 resulting from bioirrigation, bioturbation, and bottom turbidity currents. The profiles of
426 dissolved and solid phase geochemical constituents in the sediment provide indications as to
427 specific diagenetic reactions prevailing (Froelich et al., 1979). However, reoxidation of
428 reduced inorganic compounds often mask the primary reactions involved in carbon oxidation
429 (Sørensen and Jørgensen, 1987; Hines et al., 1991). Together with the discrete geochemical
430 zonation of the electron acceptors, the independently executed metabolic rate measurements
431 (Fig. 5) allowed us to evaluate the relative contribution of each terminal electron-accepting
432 pathway with sediment depth.

433 Previous experimental studies that have quantified pathways of anaerobic carbon
434 oxidation in subtidal marine sediments have generally determined the contributions of Mn
435 and Fe reduction indirectly from the difference between rates of DIC production and sulfate
436 reduction converted to carbon equivalents (e.g., Canfield et al., 1993b; Thamdrup and
437 Canfield, 1996; Vandieken et al., 2006). The inferred rates of Mn and Fe reduction were
438 further supported by the depth distribution of metal oxides and patterns of Mn^{2+} and Fe^{2+}
439 accumulation in the pore water, but could not be verified because the accumulation of
440 particulate Mn(II) and Fe(II) – which represents the overwhelming fraction of the reduced
441 pools – was not quantified. Here, we combined the indirect approach with independent
442 determination of Mn and Fe reduction rates. Thus, we obtained two separate estimates of
443 anaerobic carbon oxidation rates; based on DIC production and on the sum of sulfate, Fe, and
444 Mn reduction converted to carbon equivalents, respectively (Table 4). At M1, within the 0 –
445 10 cm depth interval, the average ratio between total anaerobic C_{org} oxidation rate (10.7
446 $\text{mmol C m}^{-2} \text{d}^{-1}$) and the C_{org} oxidation from DIC production ($14.0 \text{ mmol C m}^{-2} \text{d}^{-1}$) was 0.77
447 (Table 4). Similarly, at D3, the average ratio between total anaerobic C_{org} oxidation (6.79
448 $\text{mmol m}^{-2} \text{d}^{-1}$) and anaerobic DIC production ($7.22 \text{ mmol m}^{-2} \text{d}^{-1}$) was 0.94. There was a good
449 agreement between the two estimates with a ratio of total anaerobic C_{org} oxidation by Mn +
450 Fe + sulfate : DIC production for individual depth intervals of 0.8 – 1.2 (Table 4) with the
451 exception at the 0 – 2 cm depth of slope site (M1) where the ratio was slightly lower, 0.66,
452 possibly due to a contribution from the C_{org} oxidation by nitrate reduction. The similarity of
453 the two estimates across all incubations spanning a range of redox conditions provides
454 confidence in our approach for calculating dissimilatory Mn and Fe reduction rates.
455 Specifically, the good agreement indicates that the underlying assumptions concerning Mn
456 adsorption and reactions of Fe(III) and sulfide are valid as first-order approximations. The
457 general agreement further supports the validity of previous determinations of dissimilatory

458 Mn and Fe reduction rates based on the difference between DIC production and SO_4^{2-}
459 reduction (Canfield et al., 1993a, 1993b; Thamdrup et al., 2000; Vandieken et al., 2006;
460 Vandieken et al., 2014).

461 To elucidate the contribution of sulfate reduction in anaerobic carbon oxidation, the SRRs
462 (Fig. 5B, 5G) were converted to carbon oxidation (Thamdrup and Canfield, 1996), and then
463 compared to the DIC production rates from anoxic bag incubation (Fig. 5C, 5H). At the slope
464 site (M1), the fraction of anaerobic C_{org} oxidation coupled to sulfate reduction increased with
465 depth from 48 % at 0 – 2 cm, to 80 % at 8 – 10 cm (Table 4). Thus, the excess C_{org} oxidation
466 in the upper layers should be coupled to other electron accepting processes. Indeed, the C_{org}
467 oxidation by Fe reduction ($0.96 \text{ mmol m}^{-2} \text{ d}^{-1}$) accounted for most of the remaining anaerobic
468 C_{org} oxidation (12 – 18 % of DIC production) at 0 – 8 cm depth, consistent with the
469 distribution of Fe(III) decreasing from $> 25 \mu\text{mol cm}^{-3}$ near the surface (Fig. 6, Table 4). Mn
470 reduction was of minor importance at M1 because of the low content of Mn oxide ($< 3 \mu\text{mol}$
471 cm^{-3}). Carbon oxidation coupled to aerobic respiration was estimated to $3.1 \text{ mmol m}^{-2} \text{ d}^{-1}$
472 corresponding to 18 % of the total aerobic + anaerobic oxidation, while the contributions of
473 Fe and sulfate reduction to this total were 12 % and 50 %, respectively (Table 4). As
474 mentioned above, nitrate reduction/denitrification may contribute part of the unexplained 19 %
475 of carbon oxidation, but most of this imbalance likely reflects the combined uncertainties in
476 the estimates of the individual pathways. Additionally, our partitioning of carbon oxidation
477 pathways could be biased towards the anaerobic electron acceptors due to the use of the
478 diffusive oxygen uptake (DOU) rather than total oxygen uptake (TOU), which will exceed
479 DOU if bioirrigation is active (Glud 2008). Bioirrigation was not determined at our sites, but
480 the pore water profiles show no indication of strong irrigation (Fig. 2). An average
481 DOU/TOU ratio of ~ 0.6 has been reported for sediments at 1.5 – 2.5 km depth (Glud 2008).
482 Using this ratio, and assuming that TOU is partitioned similarly as DOU between aerobic
483 carbon oxidation and reoxidation, aerobic carbon oxidation would account for 25 %, while Fe
484 and sulfate reduction would account for 11 % and 46 % of carbon oxidation, respectively.
485 This, the potential bias from using DOU is not expected to affect the ranking of electron
486 acceptors by quantitative importance ($\text{SO}_4^{2-} > \text{O}_2 > \text{Fe(III)}$), and, as discussed further below,
487 the partitioning of C_{org} oxidation at M1 falls within the range previously reported for
488 continental margin sediments.

489 In contrast to M1, C_{org} oxidation by sulfate reduction at the basin site (D3) accounted for
490 only a small fraction (< 11 %) of anaerobic C_{org} oxidation at 0 – 6 cm interval and it only

491 dominated carbon oxidation at 8 – 10 cm (Fig. 5H, Table 4). Oxygen and NO_3^- were depleted
492 within 3.6 mm and 1 cm depth of the sediment surface, respectively (Fig. 5F), while Mn and
493 Fe(III) oxides were abundant at 0 – 4 cm and 0– 6 cm, respectively. Consistent with the
494 abundance of electron acceptors, high rates of Mn and Fe reduction (Fig. 5I and 5J) implied
495 Mn and Fe reduction as the most significant C_{org} oxidation pathways to 6 cm depth. At 0 – 2
496 cm depth, C_{org} oxidation by aerobic respiration and Mn reduction accounted for 53 % and 43 %
497 of total C_{org} oxidation, respectively (Fig. 6). At 2 – 4 cm, Mn reduction accounted for 73 % of
498 total C_{org} oxidation and 92 % of anaerobic C_{org} oxidation (Table 4, Fig. 6). Its importance
499 decreased to 22 % at 4 – 6 cm due to lower Mn contents, while microbial Fe(III) reduction
500 here contributed 51 %, and the partitioning of sulfate reduction increased to 11 % (Fig. 6).
501 Consequently, the relative distribution of each C_{org} oxidation pathway with depth at D3 (Fig. 6)
502 matched well with the depth distribution of the respective electron acceptors (Fig. 5F).
503 Overall, within the 10 cm depth sediment interval, Mn and Fe reduction were the dominant
504 C_{org} oxidation pathways comprising 45 % and 20 % of total carbon oxidation, respectively, at
505 the Mn and Fe oxide-rich site in the center of the UB (Table 4). Correction for a potential
506 underestimation of TOU, as discussed for M1, would reduce the contributions of Mn and Fe
507 reduction slightly to 41 % and 18 %, respectively.

508 Despite the high Fe oxide content at 0 – 4 cm at D3 (Fig. 5F), no solid $\text{Fe(II)}_{(\text{oxal})}$
509 accumulation was observed at this depth range (Fig. 6). This indicates that Fe(III) reduction
510 may not occur under these Mn-oxide rich conditions. Indeed, using a combination of 16S
511 rRNA-stable isotope probing and geochemical analysis in three manganese oxides-rich
512 sediments including the UB, Vandieken et al. (2012) identified bacteria related to *Colwellia*,
513 *Oceanospillaceae* and *Arcobacter* as acetate-oxidizing bacteria that potentially reduce
514 manganese, whereas no known iron reducers were detected in the Mn-rich sediment.
515 Similarly, Thamdrup et al. (2000), in Mn oxide- rich Black Sea sediment, found that the
516 abundance of viable Fe-reducing bacteria in most probable number counts was low in
517 comparison to Mn reducers and the addition of ferrihydrite did not stimulate Fe reduction,
518 which implied that Fe reduction should be outcompeted by the Mn reduction process.

519 Nonetheless, Mn reduction estimated from the increase of Mn^{2+} at 0 – 4 cm interval at D3
520 (Fig. 6) could be due to oxidation of Fe^{2+} or sulfide. Fe^{2+} may readily react with Mn oxides
521 (Myers and Nealson, 1988; Lovley and Phillips, 1988) by the reaction $2\text{Fe}^{2+} + \text{MnO}_2 + 4\text{H}_2\text{O}$
522 $= \text{Mn}^{2+} + 2\text{Fe(OH)}_3 + 2\text{H}^+$. However, in the Mn oxide-rich sediment of the Skagerrak,
523 Canfield et al. (1993b) revealed that the addition of Ferrozine, a strong complexation agent

524 for Fe^{2+} , had no inhibitory effect on the Mn^{2+} liberation, indicating that the chemical reaction
525 of MnO_2 with Fe^{2+} generated by Fe reduction was not responsible for the accumulation of
526 Mn^{2+} . As manganese reduction is thermodynamically more favorable than iron and sulfate
527 reduction, the Mn^{2+} liberation (Fig. 3) likely resulted from dissimilatory Mn reduction.

528 Despite the anoxic conditions and nitrate depletion during the bag incubation, Mn
529 reduction rates at 0 – 2 cm depth (Fig. 5I) based on Mn^{2+} accumulation were substantially
530 lower than the rates inferred from DIC accumulation (Fig. 5H). A similar discrepancy was
531 previously observed for the uppermost part of the Mn reduction zone (Thamdrup et al., 2000),
532 and is likely explained by particularly strong sorption of Mn^{2+} to fresh Mn oxide surfaces,
533 which is not included in the adsorption coefficient used here. Low Mn^{2+} together with the
534 rapid decrease of nitrate at 0-2 cm depth at D3 (Fig. 2F, 2G) also suggested that dissolved
535 reduced manganese might act as a reducing agent for nitrate as it was suggested by Aller et al.
536 (1998) in the Panama Basin and Mogollón et al. (2016) in the deep-sea sediment of the
537 Clarion-Clerton fracture zone in the northeast equatorial Pacific.

538 Previous estimation of denitrification in 0 – 2 cm depth of the UB ranged from 0.01 to
539 $0.17 \text{ mmol N m}^{-2} \text{ d}^{-1}$ (Lee, 2009), which is equivalent to a C_{org} oxidation of 0.013– 0.213
540 $\text{mmol C m}^{-2} \text{ d}^{-1}$ using the stoichiometric equation of $4\text{H}^+ + 5\text{CH}_2\text{O} + 4\text{NO}_3^- = 5\text{CO}_2 + 2\text{N}_2 +$
541 $7\text{H}_2\text{O}$. Based on the average, the contribution of carbon oxidation by denitrification (0.11
542 $\text{mmol C m}^{-2} \text{ d}^{-1}$) should be minor at the basin site ($\leq 3\%$ of total C_{org} oxidation at 0 – 2 cm;
543 $\sim 1\%$ of integrated C_{org} oxidation). This is consistent with the general consensus that C_{org}
544 oxidation by denitrification is of little importance in most marine sediments (Sørensen et al.,
545 1979; Canfield et al., 1993a; Trimmer and Engström, 2011). Denitrification may be even
546 further suppressed in Mn-rich sediments due to competitive inhibition from Mn reduction
547 (Trimmer et al., 2013).

548

549 **4.2 C_{org} oxidation dominated by manganese reduction in the UB**

550

551 Microbial Fe reduction has been quantified directly in sediments of various coastal oceans
552 (Gribsholt et al., 2003; Kostka et al., 2002a, 2002b; Hyun et al., 2007, 2009b) and indirectly
553 in deeper continental margins (Thamdrup and Canfield, 1996; Jensen et al., 2003; Kostka et
554 al., 1999). Earlier estimation from 16 different continental margin sediments indicated that
555 Fe(III) reduction contributed 22 % on average to anaerobic carbon oxidation (Thamdrup,
556 2000). Thus, the contributions from Fe(III) reduction of 12 % and 20 % of anaerobic C_{org}

557 oxidation on the slope (M1) and in the basin (D3) of the UB (Table 4) fall in the range of the
558 previous indirect estimates.

559 Unlike Fe reduction, direct estimation of manganese reduction rates is not easy, mainly
560 because of the restriction of the process to a thin surface layer (Sundby and Silverberg, 1985),
561 the rapid reduction of manganese oxides with H_2S and Fe^{2+} (Postma, 1985; Burdige and
562 Nealson, 1986; Kostka et al., 1995; Lovley and Phillips, 1988), and the adsorption of Mn^{2+} to
563 Mn oxide surface (Canfield et al., 1993b). For that reason, only two studies, from the
564 Skagerrak and Black Sea, are available for direct comparison on the partitioning of Mn
565 reduction. The process has also been indicated to be of importance in the Panama Basin based
566 on diagenetic modeling (Aller, 1990) and at some Arctic shelf sites where it was however not
567 quantified separately from Fe reduction (Vandieken et al., 2006, Nickel et al., 2008). Mn
568 reduction was responsible for over 90 % of total C_{org} oxidation at 600 m depth in the
569 Skagerrak (Canfield et al., 1993b), and accounted for 13 – 45 % of anaerobic C_{org} oxidation
570 in the Black Sea shelf sites at 60 – 130 m of water depth (Thamdrup et al., 2000). To our
571 knowledge, this report of C_{org} oxidation dominated by Mn reduction comprising 45 % of total
572 C_{org} oxidation and 57 % of anaerobic C_{org} respiration in the center of the UB (Table 4)
573 represents the first from deep-offshore basin of the eastern Asian marginal seas.

574 The difference in partitioning of Mn reduction in C_{org} oxidation between the UB, Black
575 Sea and Skagerrak reflects the close relationship between Mn oxide content in the sediment
576 and Mn reduction (Thamdrup et al., 2000). From the vertical distribution of electron
577 acceptors (Fig. 5J) and contribution of each C_{org} oxidation pathway with depth (Fig. 6), it is
578 apparent that the availability of Mn(IV) largely controls the relative contribution to C
579 oxidation. In the Skagerrak, the Mn oxides are abundant in high content down to 10 cm depth
580 (Canfield et al., 1993b), whereas Mn oxides in the Black Sea and the Ulleung Basin were
581 enriched only down to 2 cm and 4 cm, respectively (Thamdrup et al., 2000, Fig. 2). Using the
582 available data set for the three marine sediments, we further plotted the relative contribution
583 of manganese reduction to anaerobic carbon oxidation as a function of Mn-oxides content to
584 expand data from Thamdrup et al., 2000 (Fig. 7). The plot indicates saturation kinetics with a
585 close correlation between Mn oxide content and the importance of Mn reduction at low
586 contents. Curve-fitting yields a content of MnO_2 at 50 % of contribution of manganese
587 reduction to total C_{org} oxidation (K_s) of $8.6 \mu\text{mol cm}^{-3}$ similar to the approx. $10 \mu\text{mol cm}^{-3}$
588 suggested before (Thamdrup et al., 2000). This indicates that Mn reduction can be a dominant
589 C_{org} oxidation process even at low contents of Mn oxides compared to those found at UB.

590 Manganese enrichments of this magnitude have been reported for several locations on the
591 continental margins and in deep basins (Murray et al., 1984; Gingele and Kasten, 1994;
592 Gobeil et al., 1997; Haese et al., 2000; Mouret et al., 2009; Magen et al., 2011; Macdonald
593 and Gobeil, 2012; Mewes et al., 2014) in addition to the relatively few places where
594 dissimilatory Mn reduction was already indicated to be of importance, as discussed above.
595 Thus, the process may be of more widespread significance, particularly in deep basin settings
596 such as UB that allow geochemical focusing of manganese.

597

598 **4.3 Source of high Mn oxide content**

599

600 The strong enrichment of Mn in the UB surface sediment is primarily of diagenetic origin as
601 indicated by similar Mn contents at depth in the sediment at D3 ($0.95 - 3.02 \mu\text{mol cm}^{-3}$)
602 compared to M1 ($0.36 - 3.74 \mu\text{mol cm}^{-3}$) (Fig. 2) combined with higher sediment
603 accumulation rates at the slope ($0.15 - 0.3 \text{ cm y}^{-1}$) than in the basin (0.07 cm y^{-1} ; Cha et al.,
604 2005). Thus, the burial flux of Mn, and thereby the net input assuming steady state deposition,
605 is higher at M1 than at D3. Furthermore, Mn is likely subject to geochemical focusing in the
606 basin as Mn depositing at shallower depths is reductively mobilized and incompletely
607 oxidized in the thin oxic surface layer, resulting in release to the water column and net down-
608 slope transport, as inferred in other ventilated basins (Sundby and Silverberg, 1985; Canfield
609 et al., 1993b; Schaller and Wehrli, 1997). A diagenetic source of Mn enrichment was also
610 concluded in previous studies (Yin et al., 1989; Cha et al., 2007; Choi et al., 2009). The Mn
611 remaining and being buried at M1 likely represents unreactive detrital forms to a larger extent
612 than at D3 (Cha et al., 2007). Adopting the sediment accumulation rate of 0.07 cm y^{-1} in the
613 UB determined at a station 50 km from D3 (Cha et al., 2005), the average $\text{Mn}_{(\text{DCA})}$ content of
614 $1.1 \mu\text{mol cm}^{-3}$ at 10 – 20 cm depth (Fig. 2G) corresponds to a flux for permanent burial of
615 $0.002 \text{ mmol m}^{-2} \text{ d}^{-1}$ or just 0.03 % of the Mn reduction rate (Table 3), i.e., an Mn atom is
616 recycled 3800 times before it finally gets buried – first by stripping from the particles that
617 settle to the seafloor and subsequently, over and over, by reductive dissolution of the Mn
618 oxides that form by reoxidation in the oxic surface layer (or, potentially, in the nitrate zone;
619 Aller et al., 1998; Mogollón et al., 2016). This is a much more extensive recycling than found
620 in the Mn sediment of Skagerrak (130 – 260 times; Canfield et al., 1993b). The difference
621 results mainly from a much higher burial flux of Mn (as authigenic Mn(II)) in the Skagerrak
622 ($\sim 40 \mu\text{mol cm}^{-3}$; Canfield et al., 1993b). The reason that little, if any, authigenic Mn(II) is

623 buried in the UB is not clear.

624 As noted in previous studies (Aller, 1990; Canfield et al., 1993b), high contributions of
625 Mn and Fe reduction to carbon oxidation in off-shore sediments requires physical mixing,
626 which typically occurs through bioturbation. This is also the case for the UB, where the burial
627 flux from the oxic surface layer into the Mn reduction zone corresponded to $0.4 \text{ mmol m}^{-2} \text{ d}^{-1}$
628 or 5 % of the Mn reduction rate ($213 \text{ } \mu\text{mol cm}^{-3} \times 0.07 \text{ cm y}^{-1}$). Bioturbation has previously
629 been inferred, but not quantified, from ^{210}Pb profiles in the UB (Cha, 2002), and thin
630 polychaete worms were observed during our sampling. Assuming bioturbation to be a
631 diffusive process, we estimate, in a similar manner as in the previous studies and based on the
632 average gradient in $\text{Mn}_{(\text{DCA})}$ from 0.5 – 1 to 7 – 8 cm, that the Mn reduction rate would be
633 supported at a biodiffusion coefficient of $9.5 \text{ cm}^2 \text{ y}^{-1}$. This value is 3.6 times lower than the
634 coefficient estimated for the Skagerrak (Canfield et al., 1993b) and consistent with estimates
635 for other sediments with similar deposition rates (Boudreau, 1994). Thus, it is realistic that
636 bioturbation drives Mn cycling in the UB.

637

638 **4.4 The UB as a biogeochemical hotspot**

639

640 The SRRs measured in this study ($0.43 - 4.29 \text{ mmol m}^{-2} \text{ d}^{-1}$) are higher than those measured
641 in productive systems such as the Benguela upwelling system in the Southeast Atlantic
642 (Ferdelman et al., 1999; Fossing et al., 2000), and even comparable to those reported at the
643 continental slope of the Chilean upwelling system ($2.7 - 4.8 \text{ mmol m}^{-2} \text{ d}^{-1}$) (Thamdrup and
644 Canfield, 1996) at a similar depth range of 1000 – 2500 m. The total anaerobic DIC
645 production rates at the slope ($14.0 \text{ mmol m}^{-2} \text{ d}^{-1}$) and basin site ($7.2 \text{ mmol m}^{-2} \text{ d}^{-1}$) were also
646 comparable to those measured at the same depth range of a Chilean upwelling site ($9.2 - 11.6$
647 $\text{mmol m}^{-2} \text{ d}^{-1}$) (Thamdrup and Canfield, 1996). Since rates of benthic carbon oxidation are
648 largely controlled by the supply of organic carbon (Canfield et al., 2005), a high organic
649 carbon flux reflected in the high organic carbon content ($> 2.5\%$, dry wt.) in the sediment of
650 the UB (Table 1) is likely to explain the high metabolic activities. A similar high organic
651 carbon content as in the UB is rarely found in deep-sea sediment underlying oxic bottom
652 water at depths exceeding 2000 m, except for a Chilean upwelling site (Lee et al., 2008). This
653 high organic carbon content in the UB is mainly associated with the combination of enhanced
654 biological production resulting from the formation of coastal upwelling (Hyun et al., 2009a),
655 occurrence of an intrathermocline eddy resulting in the extraordinary subsurface chlorophyll-

656 a maximum (Kim et al., 2012), high organic C accumulation rates exceeding $2 \text{ g C m}^{-2} \text{ yr}^{-1}$
657 (Lee et al., 2008), and high export production (Kim et al., 2009). In addition to the large
658 vertical sinking flux, the lateral transport of the organic matter along the highly productive
659 southeastern slope of the UB also contributes to the high organic carbon content (Lee et al.,
660 2015). Consequently, high benthic mineralization resulting from the high organic content in
661 the sediment implied that the UB is a biogeochemical hotspot where significant turnover of
662 organic matter and nutrient regeneration occur.

663 The East Seas often called as “a miniature ocean” because of the independent
664 thermohaline convection system that is driven by the high density surface water sinking (Kim
665 et al., 2001) in a manner similar to that of the Great Ocean Conveyor Belt (Broecker, 1991).
666 The turnover time (ca. 100 – 300 years) of the thermohaline circulation is shorter than that of
667 the global conveyor belt of 1000 – 2000 years (Broecker and Peng, 1982). Because of the
668 shorter time-scale, together with the relatively small volume, the East Sea is expected to be
669 much more sensitive to global environmental changes (such as global warming) compared
670 with the open oceans. In this regard, the East Sea has been considered as a natural laboratory
671 that provides a useful field for large-scale oceanographic experiments to predict the response
672 of oceans associated with long-term climatic/oceanographic changes (Kim et al., 2001). Over
673 the last two decades (1982 – 2006), a rapid increase of sea surface temperature (SST) of
674 $1.09 \text{ }^\circ\text{C}$ has been recorded in the East Sea, which is the fourth highest among the 18 large
675 marine ecosystems in the world ocean (Belkin, 2009). Increased SST reduces the solubility of
676 O_2 in the surface mixed layer and enhances stratification, which ultimately affects biological
677 production in the water column and suppresses transport of O_2 -rich surface water into the
678 deep bottom. Indeed, recent oceanographic observations revealed that the gradual
679 deoxygenation and warming of the bottom water of the East Sea over the last 30 years have
680 resulted in an $\sim 10 \%$ decrease in dissolved oxygen and $\sim 0.04 \text{ }^\circ\text{C}$ increase in potential
681 temperature, which suggested a weakening of the deep convection system (Kim et al., 2001;
682 Gamo et al., 2011). Benthic metabolism and respiratory C_{org} oxidation coupled to various
683 TEAP in the sediments are largely controlled by the combination of O_2 content, temperature
684 and biological production overlying water column (Canfield et al., 2005). It is thus important
685 to monitor any changes in the rates and partitioning of C_{org} oxidation to better understand and
686 predict the variations of biogeochemical cycles of carbon, nutrients and metals potentially
687 associated with long-term climatic changes in the UB, the biogeochemical hotspot of the East
688 Sea.

689

690 **5. Conclusions**

691

692 Surface sediments of the Ulleung Basin (UB) in the far east Eurasian continent are
693 characterized by a high organic carbon content ($> 2.5\%$, dry wt.), high contents Fe oxides
694 (up to $100\ \mu\text{mol cm}^{-3}$), and very high contents of Mn oxides ($> 200\ \mu\text{mol cm}^{-3}$). We show that
695 microbial Mn and Fe reduction are the dominant C_{org} oxidation pathways, comprising 45 %
696 and 20 % of total C_{org} oxidation, respectively. The high Mn content results from highly
697 efficient recycling through reoxidation with very low permant burial of authigenic Mn(II)
698 phases. The basin topography may ensure that any Mn^{2+} escaping to the overlying water
699 returns to the sediment after reprecipitation. The relative importance of Mn reduction to C_{org}
700 oxidation displays saturation kinetics with respect to Mn oxide content with a low half-
701 saturation value ($8.6\ \mu\text{mol cm}^{-3}$), which further implies that Mn reduction can be a dominant
702 C_{org} oxidation process in sediments with lower MnO_2 content, and thereby that the process
703 might be more important in continental margin and deep basin sediments than previously
704 thought. Vertical distributions of the major terminal electron acceptors such as O_2 , nitrate,
705 Mn- and Fe oxides were systematically zoned with discrete sequential depletion according
706 to the order of decreasing energy yield for C_{org} oxidation, which are not sharply separated in
707 most aquatic sediments due to, e.g., sediment heterogeneity and mixing resulting from
708 bioirrigation, bioturbation, and bottom turbidity currents. High benthic mineralization
709 resulting from the high organic carbon content in the sediment implied that the UB is a
710 biogeochemical hotspot where significant turnover of organic matter and nutrient
711 regeneration occur. Over the last 30 years, the gradual deoxygenation and warming of the
712 bottom water of the East Sea have resulted in an $\sim 10\%$ decrease in dissolved oxygen and
713 $\sim 0.04\ ^\circ\text{C}$ increase in potential temperature. If this continues, the UB sediment provides with
714 an ideal natural laboratory to monitor changes in the rates and partitioning of C_{org} oxidation in
715 order to better understand the biogeochemical cycling of carbon, nutrients and metals
716 associated with long-term climatic changes.

717

718 **Author contribution**

719

720 J-H Hyun as first author and leader of the Korean research group designed the original
721 experiments and conducted most writing; S-H Kim, JS Mok, and H-Y Cho participated in

722 onboard research activities and analytical processes; V Vandieken participated in onboard
723 research and was actively involved in the discussion of the manuscript; D Lee, as project
724 manager of the EAST-1 program, paid the ship-time and has participated in discussion of the
725 results; B Thamdrup, as leader of the Danish research group, collaborated with J-H Hyun in
726 designing the experiments and writing and discussing the manuscript.

727

728 **Acknowledgements**

729 This research was a part of the projects titled Korean Long-term Marine Ecological
730 Researches (K-LTMER) and East Asian Seas Time Series-I (EAST-I) funded by the Korean
731 Ministry of Oceans and Fisheries, and was also supported by the National Research
732 Foundation of Korea (NRF-2012-013-2012S1A2A1A01030760) in collaboration with the
733 Danish Council for Independent Research and the Danish National Research Foundation
734 (DNRF53).

735

736 **References**

737

- 738 Aller, R. C. : Bioturbation and manganese cycling in hemipelagic sediments, Phil. Trans. R.
739 Soc. Lond. A 331, 51-68, 1990.
- 740 Aller, R. C., Hall, P. O. J., Rude, P. D., and Aller, J. Y. : Biogeochemical heterogeneity and
741 suboxic diagenesis in hemipelagic sediments of the Panama Basin, Deep-Sea Res. I, 45,
742 133-165, 1998.
- 743 Belkin, I. M. : Rapid warming of Large Marine Ecosystems, Prog. Oceanogr., 81, 207-213,
744 2009.
- 745 Berg, P., Risgaard-Petersen, N., and Rysgaard, S. : Interpretation shelf and slope: A
746 comparison of *in situ* microelectrode and chamber flux measurements, Limnol. Oceanogr.,
747 37, 614-629, 1998.
- 748 Boudreau, B. P. : Is burial velocity a master parameter for bioturbation?, Geochim.
749 Cosmochim. Acta, 58, 1243-1249, 1994.
- 750 Bowles, M. W., Mogollón, J. M., Kasten, S., Zabel, M., and Hinrichs, K.U. : Global rates of
751 marine sulfate reduction and implications for sub-sea-floor metabolic activities, Science,
752 344, 889-891, 2014.

753 Broecker, W. S. : The great ocean conveyor, *Oceanogr.*, 4, 79-89, 1991.

754 Broecker, W. S. and Peng, T. H. : Tracers in the sea, Lamont-Doherty Earth Observatory,
755 Palisades, NY., 1982.

756 Burdige, D. J. and Nealson, K. H. : Chemical and microbiological studies of sulfide-mediated
757 manganese reduction, *Geomicrobiol. J.*, 4, 361-387, 1986.

758 Canfield, D. E., Jørgensen, B. B., Fossing, H., Glud, R., Gundersen, J., Rasing, N. B.,
759 Thamdrup, B., Hansen, J. W., Nielsen, L. P., and Hall, P. O. J. : Pathways of organic
760 carbon oxidation in three continental margin sediments, *Mar. Geol.*, 113, 27-40, 1993a.

761 Canfield, D. E., Thamdrup, B., and Hansen, J. W. : The anaerobic degradation of organic
762 matter in Danish coastal sediments: iron reduction, manganese reduction, and sulfate
763 reduction, *Geochim. Cosmochim. Acta*, 57, 3867-3883, 1993b.

764 Canfield, D. E., Thamdrup, B., and Kristensen, E. (Eds.) : *Aquatic geomicrobiology*, Elsevier,
765 San Diego, 640 pp., 2005.

766 Cha, H. J., Choi, M. S., Lee, C.-B., and Shin, D.-H. : Geochemistry of surface sediments in
767 the southwestern East/Japan Sea, *J. Asian Earth Sci.*, 29, 685-697, 2007.

768 Cha, H. J., Lee, C. B., Kim, B. S., Choi, M. S., and Ruttenger, K. C. : Early diagenetic
769 redistribution and burial of phosphorus in the sediments of the southwestern East Sea
770 (Japan Sea), *Mar. Geol.*, 216, 127-143, 2005.

771 Cha, H. J. : Geochemistry of surface sediments and diagenetic redistribution of phosphorus in
772 the southwestern East Sea, PhD thesis, Seoul National Univ., Seoul, Korea, 190 pp., 2002.

773 Choi, Y. J., Kim, D. S., Lee, T. H., and Lee, C. B. : Estimate of manganese and iron oxide
774 reduction rates in slope and basin sediments of Ulleung Basin, East Sea, *J. Korean Soc.*
775 *Oceanogr.*, 14, 127-133, 2009.

776 Chough, S. K., Lee, H. J., and Yoon, S. H. (Eds.) : *Marine Geology of Korean Seas* (2nd
777 edition), Elsevier, Amsterdam, 2000.

778 Cline, J. D. : Spectrophotometric determination of hydrogen sulfide in natural waters, *Limnol.*
779 *Oceanogr.*, 14, 454-458, 1969.

780 D'Hondt, S., Inagaki, F., Zarikian, C. A., Abrams, L. J., Dubois, N., Engelhardt, T., Evans,
781 H., Ferdelman, T., Gribsholt, B., Harris, R. N., Hoppie, B. W., Hyun, J.-H. et al. :
782 Presence of oxygen and aerobic communities from sea floor to basement in deep-sea
783 sediments, *Nature Geosci.*, 8, 299-304, 2015.

784 Ferdelman, T. G., Fossing, H., Neumann, K., and Schulz, H. D. : Sulfate reduction in surface
785 sediments of the southeast Atlantic continental margin between 15°38'S and 27°57'S

786 (Angola and Namibia), *Limnol. Oceanogr.*, 44, 650-661, 1999.

787 Fossing, H., Ferdelman, T. G., and Berg, P. : Sulfate reduction and methane oxidation in
788 continental margin sediments influenced by irrigation (South-East Atlantic off Namibia),
789 *Geochim. Cosmochim. Acta*, 64, 897-910, 2000.

790 Fossing, H. and Jørgensen, B. B. : Measurement of bacterial sulfate reduction in sediments:
791 evaluation of a single-step chromium reduction method, *Biogeochem.* 8, 205-222, 1989.

792 Froelich, P. N., Klinkhammer, G.P., Bender, M.L., Luedtke, N.A., Heath, G.R., Cullen, D.,
793 Dauphin, P., Hammond, D., Hartman, B., and Maynard, V. : Early oxidation of organic
794 matter in pelagic sediments of the eastern equatorial Atlantic: suboxic diagenesis,
795 *Geochim. Cosmochim. Acta*, 43, 1075-1090, 1979.

796 Gamo, T. : Dissolved oxygen in the bottom water of the Sea of Japan as a sensitive alarm for
797 global climatic change, *Trend Anal.Chem.*, 30, 1308-1319, 2011.

798 Gamo, T., Nakayama, N., Takahata, N., Sano, Y., Zhang, J., Yamazaki, E., Taniyasu, S., and
799 Yamashita, N. : The Sea of Japan and its unique chemistry revealed by time-series
800 observations over the last 30 Year, *Monogr. Environ. Earth Planets*, 2, 1-22, 2014.

801 Gingele, F. X. and Kasten, S. : Solid-phase manganese in Southeast Atlantic sediments
802 Implications for the paleoenvironment, *Mar. Geol.*, 121, 317-332, 1994.

803 Glud, R. N. : Oxygen dynamics of marine sediments, *Mar. Biol. Res.*, 4, 243-289, 2008.

804 Gobeil, C, Macdonald, R. W.,and Sundby, B. : Diagenetic separation of cadmium and
805 manganese in suboxic continental margin sediments, *Geochim. Cosmochim. Acta*, 61,
806 4647-4654, 1997.

807 Gribsholt, B., Kostka, J. E., and Kristensen, E. : Impact of fiddler crabs and plant roots on
808 sediment biogeochemistry in a Georgia saltmarsh, *Mar. Ecol. Prog. Ser.*, 259, 237-251,
809 2003.

810 Haese, R. R., Schramm, J., Rutgers Van Der Loeff, M. M., and Schulz, H. D. : A
811 comparative study of iron and manganese diagenesis in continental slope and deep
812 seabasins sediments off Uruguay (SW Atlantic), *Int. J. EarthSci.*, 88, 619-629, 2000.

813 Hall, P. O. and Aller, R.C. : Rapid small-volume, flow injection analysis for CO₂ and NH₄⁺ in
814 marine and freshwaters, *Limnol. Oceanogr.*, 37, 113-119, 1992.

815 Hansen, C., Zabel, M., and Schulz, H. N. : Benthic cycling of oxygen, nitrogen, and
816 phosphorus, in: *Marine Geochemistry*, edited by: Schulz, H. D. and Zabel, M., Springer-
817 Verlag, Berlin, Heidelberg, NY, 207-240, 2006.

818 Hansen, J. W., Thamdrup, B., and Jørgensen, B. B. : Anoxic incubation of sediment in gas-

819 tight plastic bags: a method for biochemical process studies, *Mar. Ecol. Prog. Ser.*, 208,
820 273-282, 2000.

821 Hines, M. E., Bzylinski, D. A., Tugel, J. B., and Lyons, W. B. : Anaerobic microbial
822 biogeochemistry in sediments from two basins in the Gulf of Maine: evidence for iron and
823 manganese reduction, *Estuar. Coast. Shelf Sci.*, 32, 313-324, 1991.

824 Hyun, J.-H., Kim, D., Shin, C.-W., Noh, J.-H., Yang, E.-J., Mok, J.-S., Kim, S.-H., Kim, H.-
825 C., and Yoo, S. : Enhanced phytoplankton and bacterioplankton production coupled to
826 coastal upwelling and an anticyclonic eddy in the Ulleung basin, East Sea, *Aquat. Microb.
827 Ecol.*, 54, 45-54, 2009a.

828 Hyun, J.-H., Mok, J.-S., Cho, H.-Y., Kim, S.-H., and Kostka, J. E. : Rapid organic matter
829 mineralization coupled to iron cycling in intertidal mud flats of the Han River estuary,
830 Yellow Sea, *Biogeochem.*, 92, 231-245, 2009b.

831 Hyun, J.-H., Mok, J.-S., You, O.-R., Kim, D., and Choi, D. L.: Variations and controls of
832 sulfate reduction in the continental slope and rise of the Ulleung basin off the southeast
833 Korean upwelling system in the East Sea, *Geomicrobiol. J.*, 27, 1-11, 2010.

834 Hyun, J.-H., Smith, A. C., and Kostka, J. E. : Relative contributions of sulfate- and iron(III)
835 reduction to organic matter mineralization and process controls in contrasting habitats of
836 the Georgia saltmarsh, *Appl. Geochem.*, 22, 2637-2651, 2007.

837 Jahnke, R. A., Reimers, C. E., and Craven, D. B. : Intensification of recycling of organic
838 matter at the sea floor near ocean margins, *Nature*, 348, 50-54, 1990.

839 Jahnke, R. A. and Jahnke, D. B. : Rates of C, N, P and Si recycling and denitrification at the
840 US mid-Atlantic continental slope depocenter, *Deep-Sea Res. I*, 47, 1405-1428, 2000.

841 Jahnke, R. A., Emerson, S. R., and Murray, J. W. : A model of oxygen reduction,
842 denitrification, and organic matter mineralization in marine sediments, *Limnol. Oceanogr.*,
843 27, 610-623, 1982.

844 Jensen, M. M., Thamdrup, B., Rysgaard, S., Holmer, M., and Fossing, H. : Rates and
845 regulation of microbial iron reduction in sediments of the Baltic-North Sea transition,
846 *Biogeochem.*, 65, 295-317, 2003.

847 Jørgensen, B. B. and Kasten, S. : Sulfur cycling and methane oxidation. in: *Marine
848 Geochemistry*, edited by: Schulz, H. D. and Zabel, M., Springer-Verlag, Berlin,
849 Heidelberg, NY, 271-309, 2006.

850 Jørgensen, B. B. : A comparison of methods for the quantification of bacterial sulfate
851 reduction in coastal marine sediments, 1. Measurement with radiotracer techniques,

852 Geomicrobiol. J., 1, 11–28, 1978.

853 Jørgensen, B. B. : Bacteria and marine biogeochemistry, in: Marine Geochemistry, edited by:
854 Schulz, H. D. and Zabel, M., Springer-Verlag, Berlin, Heidelberg, NY, 169-206, 2006.

855 Jørgensen, B. B. : Mineralization of organic matter in the sea bed - the role of sulphate
856 reduction, Nature, 296, 643-645, 1982.

857 Jørgensen, B. B. and Revsbech, N. P. : Diffusive boundary layers and the oxygen uptake of
858 sediments and detritus, Limnol. Oceanogr., 30, 111-122, 1985.

859 Kang, D. J., Lee, D. S., and Kim, K.-R. : The East Sea (Sea of Japan), in: Carbon and nutrient
860 fluxes in continental margins, edited by: Liu, K.-K., Atkinson, L., Quiñones, R. A., and
861 Talaue-MaManus, L., Springer-Verlag, Berlin, Heidelberg, 383-394, 2010.

862 Kim K, Kim K.-R., Min, D. H., Volkov, Y., Yoon, J.-H., Takematsu, M. : Warming and
863 structural changes in the East Sea (Japan) Sea: a clue to future changes in the global
864 oceans?, Geophys. Res. Lett., 28, 3293-3296, 2001.

865 Kim, D., Choi, M.-S., Oh, H.-Y., Kim, K. H., and Noh, J.-H. : Estimate of particulate organic
866 carbon export flux using $^{234}\text{Th}/^{238}\text{U}$ disequilibrium in the southwestern East Sea during
867 summer, (The Sea) J. Kor. Soc. Oceanogr., 14, 1-9, 2009.

868 Kim, D., Yang, E.J., Kim, K. H., Shin, C.-W., Park, J., Yoo, S. J., and Hyun, J.-H. : Impact of
869 an anticyclonic eddy on the summer nutrient and chlorophyll a distributions in the Ulleung
870 Basin, East Sea (Japan Sea), ICES J. Marine Science, 69, 23-29, 2012.

871 Kostka, J. E., Gribsholt, B., Petrie, E., Dalton, D., Skelton, H., and Kristensen, E. : The rates
872 and pathways of carbon oxidation in bioturbated saltmarsh sediments, Limnol. Oceanogr.,
873 47, 230-240, 2002a.

874 Kostka, J. E., Roychoudhury, A., and Van Cappellen, P. : Rates and controls of anaerobic
875 microbial respiration across spatial and temporal gradients in saltmarsh sediments,
876 Biogeochem, 60, 49–76, 2002b.

877 Kostka, J. E., Thamdrup, B., Glud, R. N., and Canfield, D. E. : Rates and pathways of carbon
878 oxidation in permanently cold Arctic sediments, Mar. Ecol. Prog. Ser., 180, 7-21, 1999.

879 Kostka, J. E., Luther, G. W., and Nealson, K. H. : Chemical and biological reduction of
880 Mn(III)-pyrophosphate complexes – potential importance of dissolved Mn(III) as an
881 environmental oxidant, Geochim. Cosmochim. Acta, 59, 885-894, 1995.

882 Lee, J. S., An, S.-U., Park, Y.-G., Kim, E., Kim, D., Kwon, J. N., Kang, D.-J., and Noh, J.-H. :
883 Rates of total oxygen uptake of sediments and benthic nutrient fluxes measured using an
884 in situ autonomous benthic chamber in the sediment of the slope off the southwestern part

885 of the Ulleung Basin, East Sea, *Ocean Sci. J.*, 50, 581-588, 2015.

886 Lee, J.: Importance of nitrate reduction in coastal and deep-sea sediments, MS thesis,
887 Department of Marine Science Graduate School, Pusan National University, Korea, 86 pp.,
888 2009.

889 Lee, T., Hyun, J.-H., Mok, J. S., and Kim, D. : Organic carbon accumulation and sulfate
890 reduction rates in slope and basin sediments of the Ulleung basin, East/Japan Sea, *Geo.*
891 *Mar. Lett.* 28, 153-159, 2008.

892 Li, Y. H. and Gregory, S. : Diffusion of ions in sea water and deep sea sediments. *Geochim.*
893 *Cosmochim. Acta*, 38, 703-714, 1974.

894 Liu, K.-K., Atkinson, L., Quiñones, R. A., and Talaue-MaManus, L. : Biogeochemistry of the
895 continental margins, in: Carbon and nutrient fluxes in continental margins, edited by: Liu,
896 K.-K., Atkinson, L., Quiñones, R. A., and Talaue-MaManus, L., Springer-Verlag, Berlin,
897 Heidelberg, 3-24, 2010.

898 Lovley, D. R. and Phillips, E. J. P. : Competitive mechanisms for inhibition of sulfate
899 reduction and methane production in the zone of ferric iron reduction in sediments, *Appl.*
900 *Environ. Microbiol.*, 53, 2636-2641, 1987.

901 Lovley, D. R. and Phillips, E. J. P. : Manganese inhibition of microbial iron reduction in
902 anaerobic sediments, *Geomicrobiol. J.*, 6, 145-155, 1988.

903 Luther III, G. W. : Acid volatile sulfide – A comment, *Mar. Chem.*, 97, 198-205, 2005.

904 Macdonald, R. W. and Gobeil, C. : Manganese sources and sinks in the Arctic Ocean with
905 reference to periodic enrichments in basin sediments, *Aquat. Geochem.*, 18, 565-591, 2012.

906 Madison, S., Tebo, B. M., Mucci, A., Sundby, B., and Luther III, G. W. : Abundant
907 porewater Mn(III) is a major component of the sedimentary redox system, *Science*, 341,
908 875-878, 2013.

909 Magen, C., Mucci, A., and Sundby, B. : Reduction rates of sedimentary Mn and Fe oxides: an
910 incubation experiment with Arctic Ocean sediments, *Aquat. Biogeochem.*, 17, 629-643,
911 2011.

912 Melton, E. D., Swanner, E. D., Behrens, S., Schmidt, C., and Kappler, A. : The interplay of
913 microbially mediated and abiotic reactions in the biogeochemical Fe cycle, *Nature Rev.*
914 *Microbiol.*, 12, 797-808, 2014.

915 Mewes, K., Mogollón, J. M., Picard, A., Rühlemann, C., Eisenhauer, A., Kuhn, T., Ziebis, W.,
916 and Kasten, S. : Diffusive transfer of oxygen from seamount basaltic crust into overlying
917 sediments: an example from the Clarion-Clipperton Fracture Zone, *Earth Planet. Sci. Lett.*,

918 433, 215-225, 2016.

919 Mewes, K., Mogollón, J. M., Picard, A., Rühlemann, C., Kuhn, T., Nöthen, K., and Kasten,
920 S. : Impact of depositional and biogeochemical processes on small scale variations in
921 nodule abundance in the Clarion-Clipperton Fracture Zone, *Deep-Sea Res. I*, 91, 125-141,
922 2014.

923 Meyers, C. and Nealson, K. H.: Microbial reduction of manganese oxides: Interactions with
924 iron and sulfur, *Geochim. Cosmochim. Acta*, 52, 2727-2732, 1988.

925 Mogollón, J. M., Mewes, K., and Kasten, S. : Quantifying manganese and nitrogen cycle
926 coupling in manganese-rich, organic carbon-starved marine sediments: examples from the
927 Clarion-Clipperton fracture zone, *Geophys. Res. Lett.*, 43, doi:10.1002/2016GL069117,
928 2016.

929 Mouret, A., Anschutz, P., Lecroart, P., Chaillou, G., Hyacinthe, C., Deborde, J., Jorissen,
930 F., Deflandre, B., Schmidt, S., and Jouanneau, J.-M. : Benthic geochemistry of manganese
931 in the Bay of Biscay, and sediment mass accumulation rate, *Geo. Mar. Lett.* 29, 133-149,
932 2009.

933 Murray, J. W., Balistrieri, L. S., and Paul, B. : The oxidation state of manganese in
934 marine sediments and ferromanganese nodules, *Geochim. Cosmochim. Acta*, 48, 1237-
935 1247, 1984.

936 Nickel, M., Vandieken, V., Brüchert, V., and Jørgensen, B. B. : Microbial Mn(IV) and Fe(III)
937 reduction in northern Barents Sea sediments under different conditions of ice cover and
938 organic carbon deposition, *Deep-Sea Res. II*, 55, 2390-2398, 2008.

939 Parsons, T. R., Maita, Y., and Lalli, C. M. (Eds.) : A manual of chemical and biological
940 methods for seawater analysis, Pergamon Press, Oxford, 173 pp., 1984.

941 Phillips, E. J. P. and Lovley, D. R. : Determination of Fe(III) and Fe(II) in oxalate extracts of
942 sediment, *Soil Sci. Soc. Am. J.*, 51, 938-941, 1987.

943 Postma, D. : Concentration of Mn and separation from Fe in sediments – I. Kinetics and
944 stoichiometry of the reaction between birnessite and dissolved Fe(II) at 10°C, *Geochim.*
945 *Cosmochim. Acta*, 49, 1023-1033, 1985.

946 Pyzik, A. E. and Sommer, S. E. : Sedimentary iron monosulfide: kinetics and mechanisms of
947 formation, *Geochim. Cosmochim. Acta*, 45, 687-698, 1981.

948 Rasmussen, H. and Jørgensen, B. B. : Microelectrode studies of seasonal oxygen uptake in a
949 coastal sediment: role of molecular diffusion, *Mar. Ecol. Prog. Ser.*, 81, 289-303, 1992.

950 Rickard, D. and Morse, J. W. : Acid volatile sulfur (AVS), *Mar. Chem.*, 97, 141-107, 2005.

951 Romankevich, E. A. : Geochemistry of organic matter in the ocean, Springer-Verlag, Berlin,
952 Heidelberg, NY, Tokyo, 334 pp., 1984.

953 Schaller, T. and Wehrli, B. : Geochemical-focusing of manganese in lake sediments –An
954 indicator of deep-water oxygen conditions, *Aquat. Geochem.*, 2, 359-378, 1997.

955 Slomp, C. P., Mort, H. P., Jilbert, T., Reed, D. C., and Gustafsson, B. G. : Coupled dynamics
956 of iron and phosphorus in sediments of an oligotrophic coastal basin and the impact of
957 anaerobic oxidation of methane, *PLoS ONE*, 8, e62386, 2013.

958 Sørensen, J. W. and Jørgensen, B. B. : Early diagenesis in sediments from Danish coastal
959 waters: Microbial activity and Mn-Fe-S geochemistry, *Geochim. Cosmochim. Acta*, 51,
960 1583-1590, 1987.

961 Sørensen, J. W., Jørgensen, B. B., and Revsbech, N. P. : A comparison of oxygen, nitrate and
962 sulfate respiration in a coastal marine sediment, *Microb. Ecol.*, 5, 105-115, 1979.

963 Stookey, L. L. : Ferrozine - a new spectrophotometric reagent for iron, *Anal. Chem.* 42, 779-
964 781, 1970.

965 Sundy, B. and Silverberg, N. : Manganese fluxes in the benthic boundary layer, *Limnol.*
966 *Oceanogr.*, 30, 372-381, 1985.

967 Thamdrup, B. and Canfield, D. E. : Pathways of carbon oxidation in continental margin
968 sediments off central Chile, *Limnol. Oceanogr.* 41, 1629-1650, 1996.

969 Thamdrup, B. and Dalsgaard, T. : The fate of ammonium in anoxic manganese oxide-rich
970 marine sediment, *Geochim. Cosmochim. Acta*, 64, 4157-4164, 2000.

971 Thamdrup, B., Rosselló-Mora, R., and Amann, R. : Microbial manganese and sulfate
972 reduction in Black Sea shelf sediments, *Appl. Environ. Microbiol.*, 66, 2888-2897, 2000.

973 Thamdrup, B. : Bacterial manganese and iron reduction in aquatic sediments, *Adv. Microb.*
974 *Ecol.* 16, 41-84, 2000.

975 Trimmer, M. and Engström, P. : Distribution, activity, and ecology of anammox bacteria in
976 aquatic environments, in: *Nitrification*, edited by: Ward, B. B., Arp, D. J., and Klotz, M. G.,
977 ASM Press, Washington, DC, 201-235, 2011.

978 Trimmer, M., Engström, P., and Thamdrup, B. : Stark contrast in denitrification and anammox
979 across the deep Norwegian Trench in the Skagerrak, *Appl. Environ. Microbiol.*, 79, 7381-
980 7389, 2013.

981 Vandieken, V., Pester, M., Finke, N., Hyun, J.-H., Friedrich, M. W., Loy, A., and Thamdrup,
982 B. : Identification of acetate-oxidizing manganese-reducing bacteria in three manganese
983 oxide-rich marine sediments by stable isotope probing, *ISME J.*, 6, 2078-2090, 2012.

- 984 Vandieken, V., Finke, N., and Thamdrup, B. : Hydrogen, acetate, and lactate as electron
985 donors for microbial manganese reduction in a manganese-rich coastal marine sediment,
986 FEMS Microbiol Ecol., 87, 733-745, 2014.
- 987 Vandieken, V., Nickel, M., and Jørgensen, B. B. : Carbon mineralization in Arctic sediments
988 northeast of Svalbard: Mn(IV) and Fe(III) reduction as principal anaerobic respiratory
989 pathways, Mar. Ecol. Prog. Ser., 322, 15-27, 2006.
- 990 Walsh, J. J. : Importance of continental margins in the marine biogeochemical cycling of
991 carbon and nitrogen, Nature, 350, 53-55, 1991.
- 992 Yamada, K., Ishizaka, J., and Nagata, H. : Spatial and temporal variability of satellite primary
993 production in the Japan Sea from 1998 to 2002, J. Oceanogr., 61, 857-869, 2005.
- 994 Yin, J. H., Kajiwara, Y., and Fujii, T. : Distribution of transition elements in surface
995 sediments of the southwestern margin of Japan Sea. Geochem. J., 23, 161-180, 1989.
- 996 Yoo, S. and Park, J. S. : Why is the southwest the most productive region of the East Sea/Sea
997 of Japan?, J. Mar. Syst., 78, 301-315, 2009.

998

999 Table 1. Environmental settings and sediment characteristics

Environmental parameter	M1 (Continental slope)	D3 (Center of the basin)
Latitude	36° 10' N	37° 00' N
Longitude	130° 10' E	131° 00' E
Water depth (m)	1,453	2,154
Sediment temperature (°C)	1.3	0.6
Pore-water salinity (psu)	34.2	34.8
Water content (%)	85 (± 3.1)	77 (± 1.8)
Porosity	0.95 (± 0.03)	0.86 (± 0.01)
Density (g cm ⁻³)	1.10 (± 0.02)	1.12 (± 0.02)
Total organic carbon (% , dry wt.)	3.96 (± 0.27)	2.66 (± 0.09)
Total organic nitrogen (% , dry wt.)	0.38 (± 0.01)	0.35 (± 0.01)

Numbers in parenthesis indicate ± 1SD of triplicate samples.

1000

1001

1002

1003
1004
1005
1006

Table 2. Oxygen penetration depth (OPD), diffusive oxygen utilization (DOU) rate and O₂ consumption rate by aerobic respiration and re-oxidation of reduced inorganic compounds (RIC) in the pore water.

Station	OPD (mm)	DOU (mmol O ₂ m ⁻² d ⁻¹)	O ₂ consumption (mmol O ₂ m ⁻² d ⁻¹) by	
			Aerobic respiration	Re-oxidation of RIC
M1	3.2 (± 0.20)	7.12 (± 1.36)	4.04 (± 2.03)	3.07 (± 0.68)
D3	3.6 (± 0.03)	5.95 (± 0.16)	2.53 (± 0.72)	3.42 (± 0.58)

1007
1008
1009
1010

Values represent averages ± 1SD (*n* = 3)

1011 Table 3. Depth integrated rates ($\text{mmol m}^{-2} \text{d}^{-1}$) of Mn reduction, Fe reduction, and sulfate reduction and the partitioning of abiotic and
 1012 microbial Fe(III) reduction in total Fe(III) reduction with depth.

St.	Depth Interval (cm)	SO_4^{2-} Red	Mn Red	^(a) Total Fe(III) Red	Fe reduction by		Fe Red _(Microbial) / Fe Red _(Abiotic)
					^(a) Abiotic Fe Red	^(a) Microbial Fe Red	
M1	0 – 2	1.35	0.04	4.75	0.90	3.86	4.28
	2 – 4	1.04	-	3.02	0.70	2.33	3.33
	4 – 6	0.84	-	1.58	0.56	1.21	2.16
	6 – 8	0.54	-	1.25	0.36	0.89	2.47
	8 – 10	0.53	-	0.77	0.36	0.41	1.14
	Sum (0-10)	4.30	0.04	11.4	2.88	8.70	
D3	0 – 2	0.06	^(b) 3.19	-	-	-	n.a.
	2 – 4	0.11	3.96	1.63	0.07	1.56	22.3
	4 – 6	0.13	1.05	4.80	0.09	4.71	52.3
	6 – 8	0.06	0.01	0.86	0.04	0.83	20.8
	8 – 10	0.07	0.00	0.24	0.05	0.19	3.80
	Sum (0-10)	0.43	8.21	7.53	0.25	7.29	

1013 ^(a)Stoichiometric equations were used to evaluate the relative significance of abiotic and microbial Fe reduction:

1014 Abiotic reduction of Fe(III) by sulfide oxidation, $3\text{H}_2\text{S} + 2\text{FeOOH} = 2\text{FeS} + \text{S}^0 + 4\text{H}_2\text{O}$; Microbial Fe(III) reduction = Total Fe(III) reduction – abiotic Fe(III) reduction.

1015 ^(b)back-calculated from the C oxidation by Mn reduction in the 0 – 2 cm interval in Table 5 using the stoichiometric equation, $2\text{MnO}_2 + \text{CH}_2\text{O} + \text{H}_2\text{O} = 2\text{Mn}^{2+} + \text{HCO}_3^- + 3\text{OH}^-$.

1016 ‘-’ indicates that the process does not occur or is regarded as negligible at the depth interval based on the OPD for aerobic respiration and geochemical profiles or anoxic
 1017 bag incubations for Mn(IV) and Fe(III) reduction

1018 ‘n.a.’ indicates that data are not available.

1019

1020

1021

Table 4. Organic carbon (C_{org}) oxidation ($mmol C m^{-2} d^{-1}$) by each C_{org} oxidation pathway, and its partitioning in total C_{org} oxidation (% Total C_{ox}) and anaerobic C_{org} oxidation (% Anaerobic C_{org} ox) at each depth interval within 10 cm of the sediment. Mn Red, Mn reduction; Fe Red, Fe reduction; and SO_4^{2-} Red, sulfate reduction

St.	Depth Interval (cm)	C_{org} oxidation measured by		^(c) Total C_{org} oxidation (DOU + DIC)	Anaerobic C_{org} oxidation by dissimilatory			Total anaerobic C_{org} oxidation (Mn Red + Fe Red + SO_4^{2-} Red)	Total Anaerobic C_{org} oxidation / Anoxic DIC production
		^(a) DOU (Aerobic respiration)	^(b) DIC prod. (Anaerobic respiration)		^(d) Mn Red	^(d,e) Fe Red	^(d) SO_4^{2-} Red		
M1	0 – 2	3.11	5.59	8.70	0.02	0.96	2.69	3.67	0.66
	2 – 4	-	3.31	3.31	-	0.58	2.09	2.67	0.81
	4 – 6	-	2.26	2.26	-	0.26	1.67	1.93	0.85
	6 – 8	-	1.50	1.50	-	0.22	1.08	1.30	0.87
	8 – 10	-	1.37	1.37	1.37	-	0.10	1.17	0.85
	Sum (0 – 10)	3.11	14.0	17.1	0.02	2.13	8.59	10.7	0.77
	(% Total C_{org} ox) (% Anaerobic C_{org} ox)	(18.1)	(81.9)	(100)	(0.13) (0.16)	(12.4) (15.2)	(50.1) (61.2)	(62.7)	
D3	0 – 2	1.94	1.72	3.66	^(f) 1.59	-	0.13	1.72	1.00
	2 – 4	-	2.72	2.72	1.98	0.39	0.22	2.58	0.95
	4 – 6	-	2.32	2.32	0.52	1.18	0.26	1.96	0.84
	6 – 8	-	0.30	0.30	0.01	0.21	0.12	0.33	1.10
	8 – 10	-	0.16	0.16	0.16	-	0.05	0.19	1.21
	Sum (0 – 10)	1.94	7.22	9.2	4.10	1.82	0.86	6.79	0.94
	(% Total C_{org} ox) (% Anaerobic C_{org} ox)	(20.6)	(78.8)	(100)	(44.8) (56.8)	(19.9) (25.2)	(9.41) (11.9)	(77.8)	

1022 ^(a) Aerobic C_{org} oxidation rate (= O_2 consumption by aerobic respiration \times (106C/138 O_2) calculated using the Redfield ratio; O_2 consumption by aerobic respiration rate (= DOU - re-oxidation
1023 rates) is calculated from Table 2 that is derived from the O_2 micro-profiles in Fig. 2.

1024 ^(b) independently measured from the DIC accumulation rate in anoxic bag incubation experiment in Fig. 6 and 7.

1025 ^(c) Total C_{org} oxidation = aerobic C_{org} oxidation + anaerobic C_{org} oxidation

1026 ^(d) C_{org} oxidation by dissimilatory Mn(IV) reduction, Fe(III) reduction, and sulfate reduction was calculated from the stoichiometric equations: $2MnO_2 + CH_2O + H_2O = 2Mn^{2+} + HCO_3^- +$
1027 $3OH^-$; $4Fe(OH)_3 + CH_2O = 4Fe^{2+} + HCO_3^- + 7OH^-$; $SO_4^{2-} + 2CH_2O = H_2S + 2HCO_3^-$, $H_2S = HS^- + H^+$

1028 ^(e) Dissimilatory Fe(III) reduction = (Total Fe(III) reduction in Fig.7) – (Abiotic Fe(III) reduction coupled to H_2S oxidation; $3H_2S + 2FeOOH = 2FeS + S^0 + 4H_2O$)

1029 ^(f) back-calculated from: DIC production rate - (C oxidation by SO_4^{2-} Red and Fe Red). See text for further discussion

1030 ‘ - ’ indicates that the process does not occur or is regarded as negligible based on the OPD for aerobic respiration and geochemical profiles or anoxic bag incubations for Mn and Fe Red.

1031

1032

Figure legends

Fig. 1. Sampling stations in the East Sea and pictures showing contrasting colors between surface sediments of the continental slope (M1) and center of the basin (D3)

Fig. 2. Concentrations of dissolved NH_4^+ , NO_3^- , Mn^{2+} and Fe^{2+} in pore water and contents of solid phase $\text{Mn}_{(\text{DCA})}$, $\text{Fe(II)}_{(\text{oxal})}$, $\text{Fe(III)}_{(\text{oxal})}$, acid volatile sulfur (AVS) and chromium reducible sulfur (CRS) in the sediment at M1 and D3.

Fig. 3. Vertical profiles of O_2 . The slashed area indicates the diffusive boundary layer in the sediment-water interface. The shaded area indicates that O_2 consumption by aerobic respiration (I and II) and re-oxidation of reduced inorganic compounds (III), respectively.

Fig. 4. Changes of concentrations of DIC, Ca^{2+} and Mn^{2+} in pore water and contents of solid phase $\text{Fe(II)}_{(\text{oxal})}$ during anoxic bag incubations of sediments from 0-2, 2-4, 4-6, and 6-8 cm depth at M1 and D3. Data obtained at 8-10 cm depth interval is not shown.

Fig. 5. Vertical distribution of terminal electron acceptors (O_2 , NO_3^- , Mn and Fe) and rates of sulfate reduction measured from whole core analyses, and rates of anaerobic carbon oxidation (DIC production rates), Mn reduction and Fe reduction measured from anoxic bag incubations in Fig. 4. C_{org} by sulfate reduction in panel C and H was calculated from the stoichiometry of 2:1 of C_{org} oxidized to sulfate reduced.

Fig. 6. Depth variations of partitioning of each carbon oxidation pathway in total carbon oxidation at M1 and D3

Fig. 7. The relative contribution of Mn reduction to anaerobic carbon oxidation as a function of the content of $\text{Mn}_{(\text{DCA})}$ at 3 different sites. BS, Black Sea (Thamdrup et al. 2000); UB, Ulleung Basin (This study); Sk, Skagerrak (Canfield et al. 1993b).

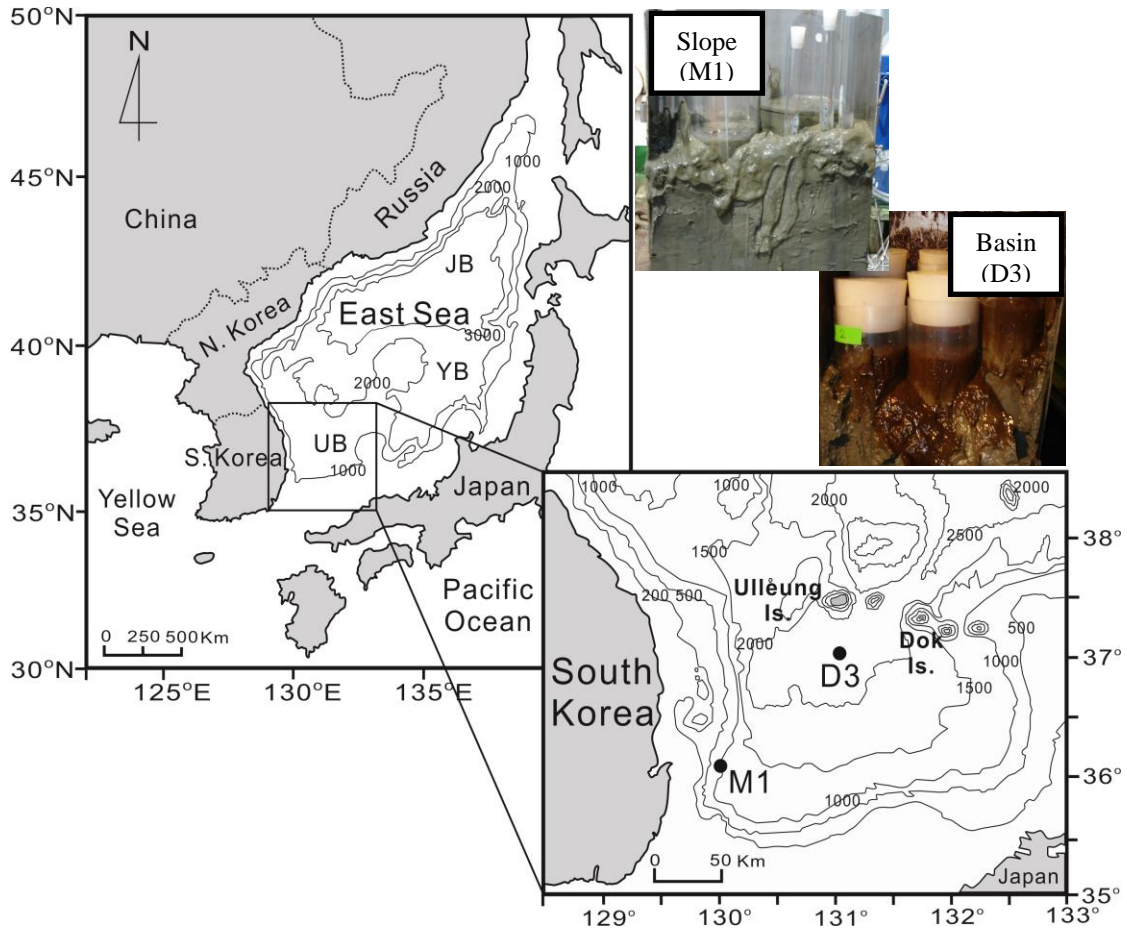
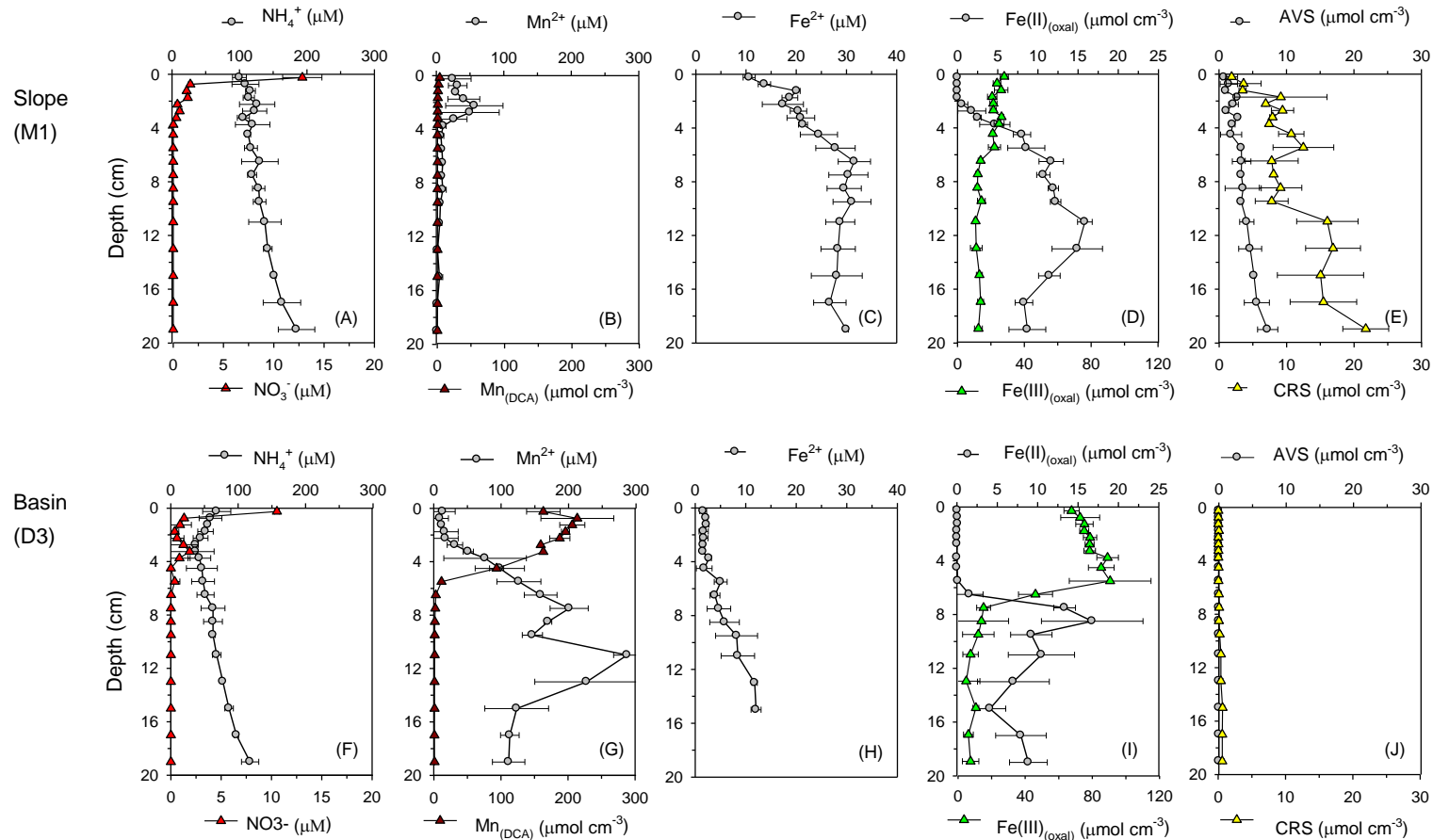


Fig. 1. Sampling stations in the East Sea and pictures showing contrasting colors between surface sediments of the continental slope (M1) and center of the basin (D3)

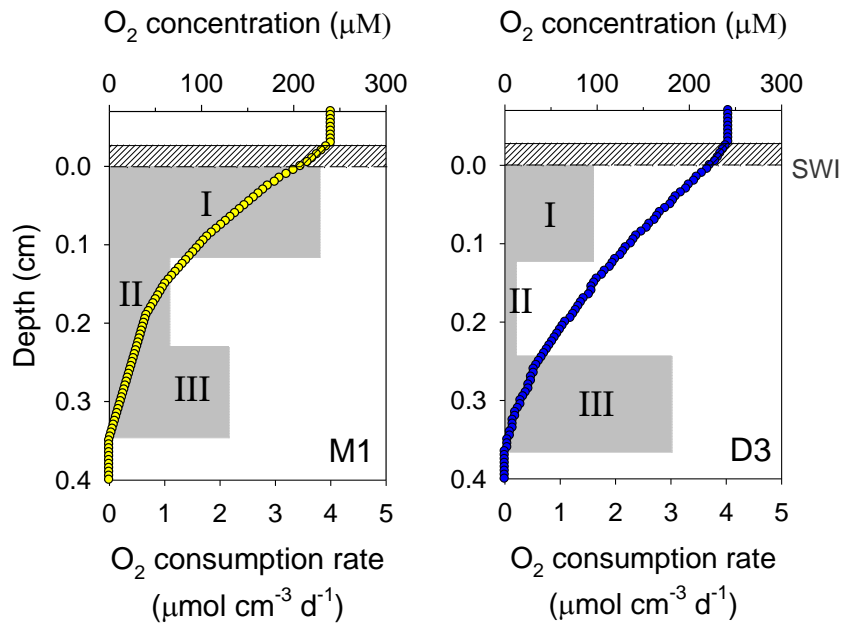
1 Hyun et al – Figure 2



2
3
4
5
6

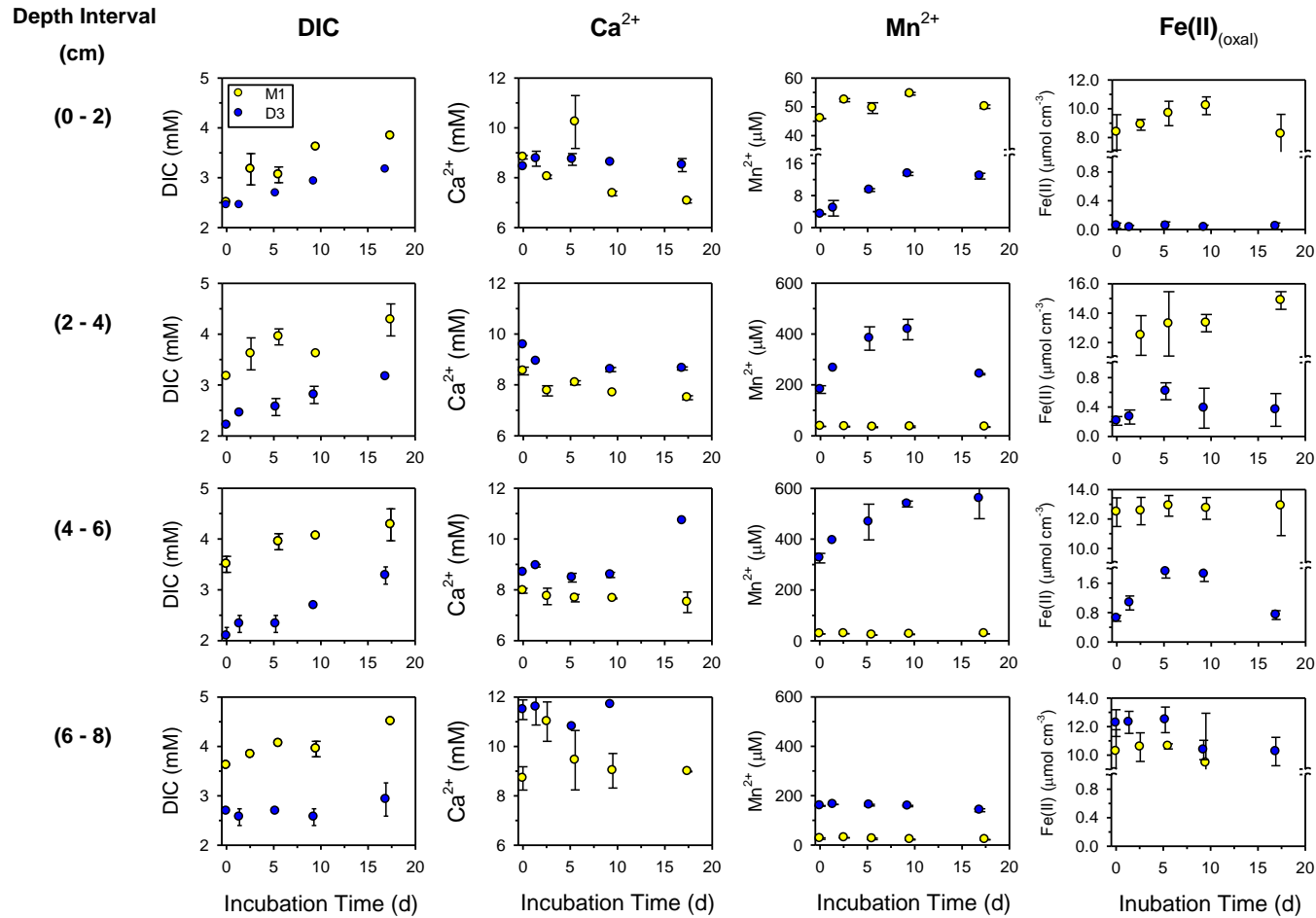
Fig. 2. Concentrations of dissolved NH_4^+ , NO_3^- , Mn^{2+} and Fe^{2+} in pore water and contents of solid phase $\text{Mn}_{(\text{DCA})}$, $\text{Fe}(\text{II})_{(\text{oxal})}$, $\text{Fe}(\text{III})_{(\text{oxal})}$, acid volatile sulfur (AVS) and chromium reducible sulfur (CRS) in the sediment at M1 and D3.

7 Hyun et al – Figure 3
8
9

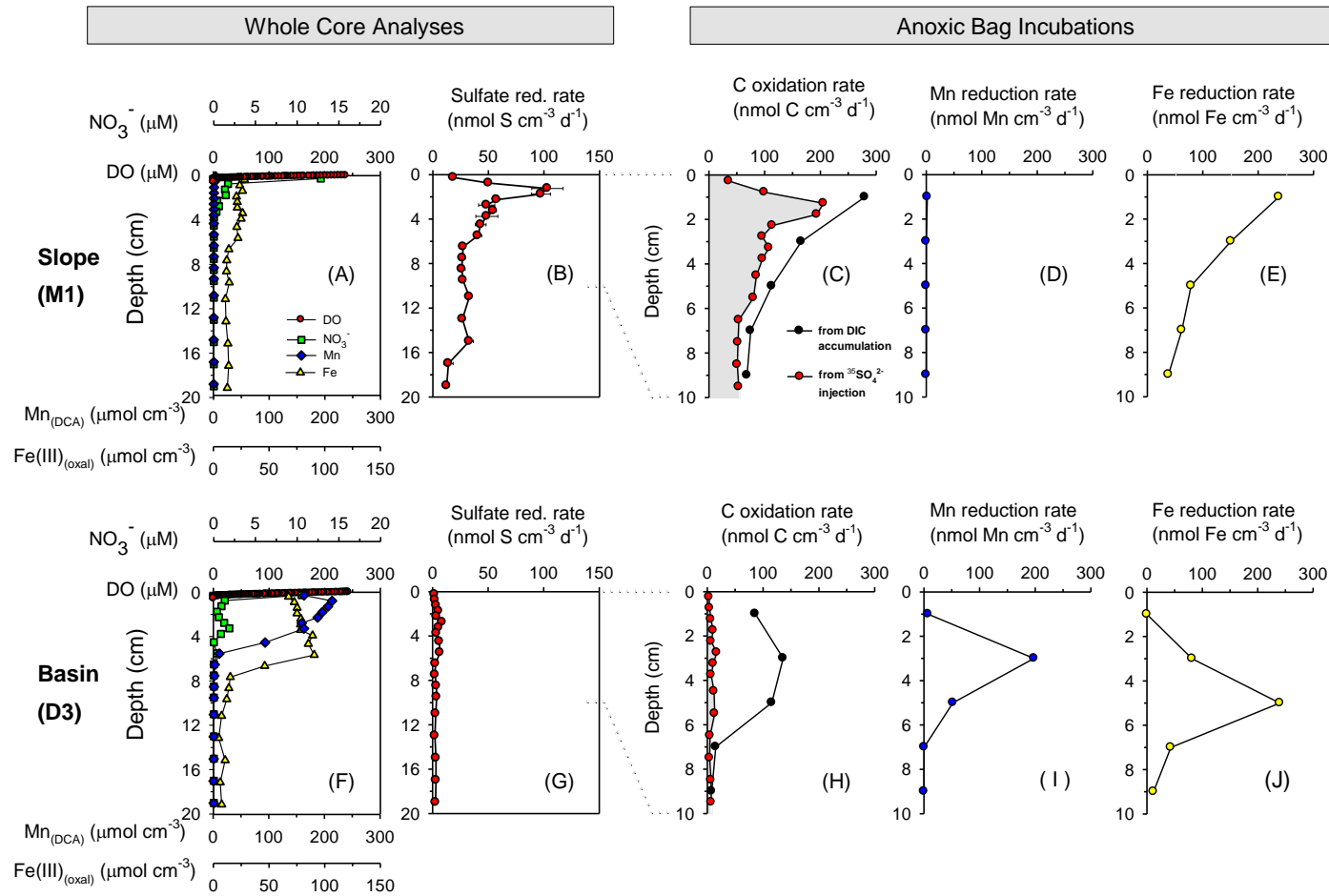


10
11
12
13
14
15
16
17
18
19
20

Fig. 3. Vertical profiles of O₂. The slashed area indicates the diffusive boundary layer in the sediment-water interface. The shaded area indicates that O₂ consumption by aerobic respiration (I and II) and re-oxidation of reduced inorganic compounds (III), respectively.

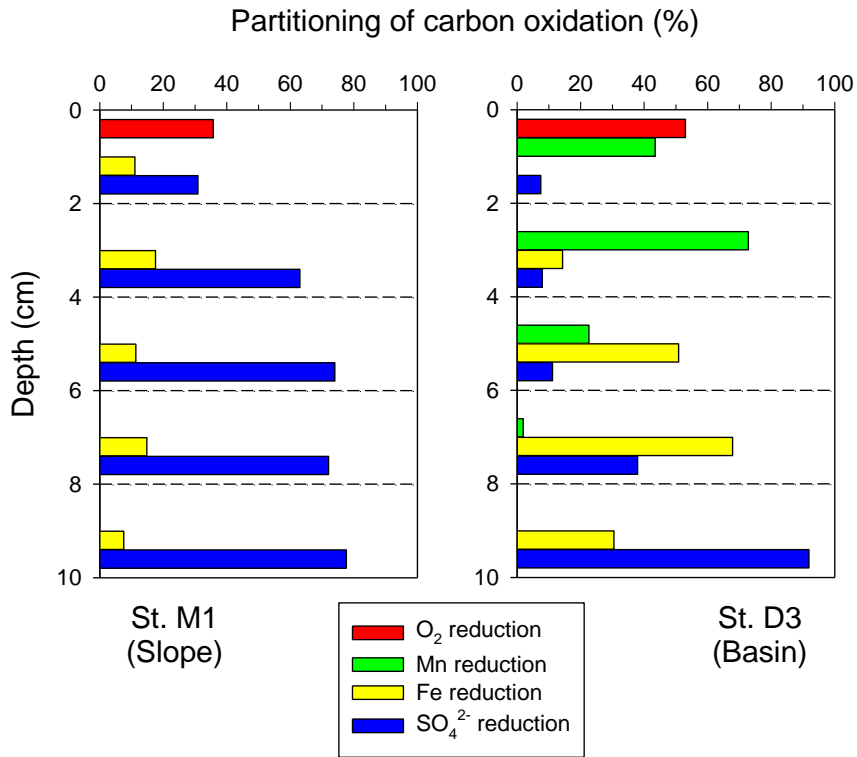


24 Fig. 4. Changes of concentrations of DIC, Ca²⁺ and Mn²⁺ in pore water and contents of solid phase Fe(II)_(oxal) during anoxic bag incubations of
 25 sediments from 0-2, 2-4, 4-6, and 6-8 cm depth at M1 and D3. Data obtained at 8-10 cm depth interval is not shown.



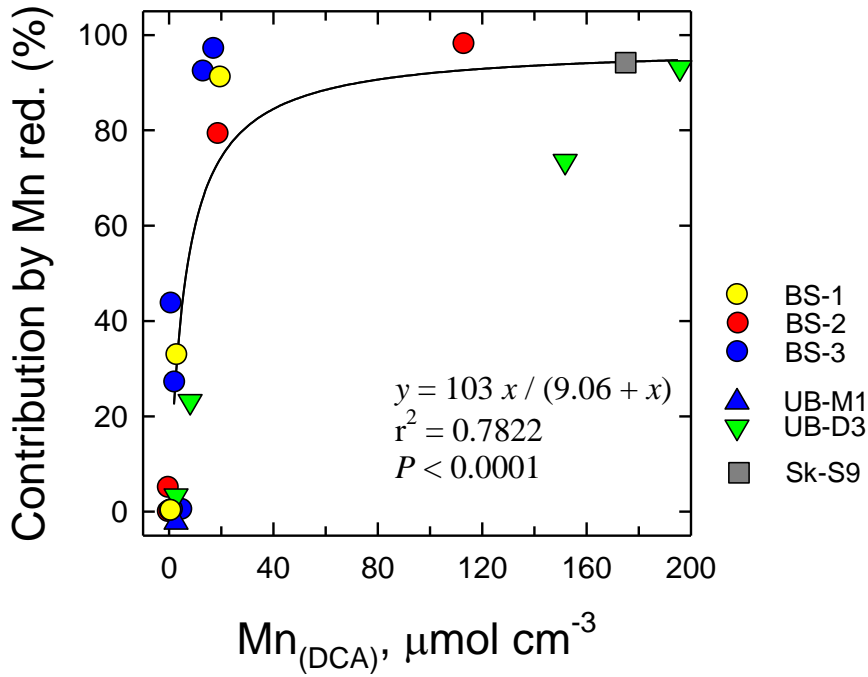
27
 28 Fig. 5. Vertical distribution of terminal electron acceptors (O_2 , NO_3^- , Mn and Fe) and rates of sulfate reduction measured from whole core analyses, and
 29 rates of anaerobic carbon oxidation (DIC production rates), Mn reduction and Fe reduction measured from anoxic bag incubations in Fig. 4. C_{org} by sulfate
 30 reduction in panel C and H was calculated from the stoichiometry of 2:1 of C_{org} oxidized to sulfate reduced.

31 Hyun et al. – Figure 6
32
33



34
35
36
37 Fig. 6. Depth variations of partitioning of each carbon oxidation pathway in total carbon
38 oxidation at M1 and D3
39

40
41 Hyun et al - Figure 7
42



43
44
45
46 Fig. 7. The relative contribution of Mn reduction to anaerobic carbon oxidation as a
47 function of the content of Mn(DCA) at 3 different sites. BS, Black Sea (Thamdrup et al.
48 2000); UB, Ulleung Basin (This study); Sk, Skagerrak (Canfield et al. 1993b).
49
50